APPENDIX D1

Modeling Brine Disposal into Monterey Bay

This page intentionally left blank

Modeling Brine Disposal into Monterey Bay

Philip J. W. Roberts, PhD, PE
Consulting Engineer
Atlanta, Georgia, USA

Final report

Prepared for
ESA | Environmental Science Associates
San Francisco, California

July 6, 2016

CONTENTS

EXECUTIVE SUMMARY

It is proposed to dispose of brine concentrate resulting from reverse osmosis (RO) seawater desalination into Monterey Bay, California. The disposal will be through an existing outfall and diffuser usually used for domestic wastewater. Previous analyses of the mixing characteristics and dilution of the effluent are updated to account for new flow scenarios, new research on the dynamics of dense jets, the internal hydraulics of the outfall, revision of the California Ocean Plan, and potential mortality of organisms due to jet-induced turbulence.

The California Ocean Plan (SWRCB, 2015) contains new requirements on concentrate disposal, in particular the definition of a brine mixing zone (BMZ) at whose boundary salinity increment limitations must be met and within which salinity must be estimated. It also requires estimates of the effect of velocity shear and turbulence on the mortality of larvae and other organisms that are entrained into the high velocity diffuser jets. New flow scenarios consisting of various combinations of brine and treated domestic effluent have also been proposed, and new data on density stratification around the diffuser have been obtained. Finally, no detailed computations of the internal flow hydraulics of the diffuser have previously been made to address the variation of flow along the diffuser and its effect on dilution.

The outfall diffuser consists of "duckbill" check valves whose opening varies with changing flow rate and it has a fixed opening in the end gate for flushing purposes. An iterative procedure was used that accounts for the flow characteristics of the valves, friction losses, and density head. The total head loss in the outfall and the flow distribution between the various ports were computed for the various flow scenarios. For dense discharges, the flow per port increases towards the diffuser end; for buoyant discharges the flows decrease. Flow variations were generally less than about ±7% from the average flow. About 5% of the total flow exits from the end gate opening. These flow variations were accounted for in the dilution simulations.

Several flow and environmental scenarios were analyzed. They consist of various combinations of brine and brine blended with secondary effluent and GWR effluent. The flow combinations occur at different times of the year and the environmental conditions that correspond to each scenario was analyzed. The most important ambient characteristics that affect dilution are the density stratification in the water column and the ambient density at the discharge depth. Density data obtained for the project (Figure 2) were analyzed and seasonal profiles obtained. The final combinations of flow and ambient conditions that were analyzed are summarized in Table 6. Zero current speed was assumed for all dilution calculations.

Dilutions for brine solutions resulting in dense effluents were first computed. For each flow scenario, the internal hydraulics were computed and the maximum and minimum flows per port and their corresponding equivalent port diameters were computed. Dilutions were calculated for each and the lowest dilution adopted. Dilution was calculated by a semi-empirical equation due to Cederwall and by the UM3 module of the US EPA model suite Visual Plumes (Table 7). The results were in close agreement and the Cederwall predictions were adopted as the most conservative. Minimum (centerline) dilutions on the seabed were generally greater than 16:1 at distances of about 10 to 30 ft from the diffuser. The salinity requirement of the Ocean Plan that the salinity increment be less than 2 ppt over natural background within 100 m from the diffuser was met in all cases. Increases in salinity are highest on the seabed, and will only be above background for a few meters above the seabed. They will be zero throughout most of the water column.

Discharges of flows that are positively buoyant were analyzed separately. Dilution and plume rise height were modeled by the modules UM3 and NRFIELD of Visual Plumes. NRFIELD is the most appropriate model and its predictions of minimum dilution were in good agreement with UM3 predictions of *average* dilution. The results are summarized in Table 8. Dilutions are generally very high, always exceeding 100:1, and the plume is usually trapped below the water surface by the ambient stratification.

For some dense flow cases, particularly when small volumes of secondary effluent are added to the brine, it is possible that dilutions may not be sufficient to achieve water quality standards. Mitigation schemes to enhance dilution for these cases were considered and analyzed, including:

1. Increase the jet velocity and decrease the density difference between the effluent and receiving water by augmenting the discharges with treated freshwater from the GWR or desalination facility.

   The effect of adding freshwater on dilution for the problematical cases are shown in Figure 18. Small additions do not substantially increase dilution. As the effluent density approaches background levels, dilution increases exponentially. The water quality requirements for these cases could be achieved by adding about 2 to 4 mgd of freshwater.

2. Vary the flow per port by either temporarily storing on site in a storage basin and pumping briefly at higher flow rates, by closing off some ports, or by opening some closed ports.

   The effect of varying the flow per port is shown in Figure 20. The dilution is relatively insensitive to flow rate. As the flow increases, the jet velocity increases and entrainment increases. However, the check valves also open offsetting this increase. The flow and heads needed to meet the water

quality requirements are excessive. Varying the flow rate is not an effective strategy for increasing dilution.

3. Discharge through upwardly inclined nozzles either by retrofitting the existing horizontal nozzles or by constructing a new dedicated brine diffuser.

   Discharge through upwardly inclined jets increases the length of dense jet trajectories and increases dilution. Jets at 60° to the horizontal (the de facto standard) were evaluated. The results are shown in Table 16. The inclined nozzles increase dilution of dense discharges substantially. All dilution requirements, including the problematical cases, would be met. The effect of retrofitting the nozzles on the dilution of positively buoyant discharges was also evaluated. The effect was small, dilutions were reduced by less than 10% compared to horizontal nozzles.

The 2015 California Ocean Plan requires an evaluation *of "...mortality that occurs due to shearing stress resulting from the facility's discharge..."* It has been suggested that planktonic organisms entrained into the high velocity turbulent jets could be subject to possibly fatal injury. Experimental evidence suggests that the main effect occurs to organisms whose size is about the same as the small-scale turbulent eddies, known as the Kolmogorov scales, which subject them to high strain rates and viscous shear stresses. The effects vary by organism; the relevant literature is summarized in Appendix C. Surveys of plankton in the vicinity of the diffuser were made and are summarized in Figure 9. As precise estimates of plankton mortality due to turbulence are not presently possible several approaches to this problem are taken.

The turbulence characteristics of jets are reviewed and turbulent length scales estimated for the various brine discharge scenarios (Table 10). The Kolmogorov scales range from about 0.012 mm near the nozzle to 2.5 mm at the jet edges at seabed impact. Exposure of larvae to jet turbulence ranges from a few seconds to minutes. The scales are smaller than or comparable to the smallest organisms of interest (Table 9) so some effects may be anticipated. The scales are somewhat smaller than those due to natural turbulence in the ocean, which is about 1 mm. Therefore, the Kolmogorov scale of the ocean is also comparable to larvae size and may cause natural mortality. The major issue is then incremental mortality due to the jets.

The total volumes in the jets where turbulent intensities are greater than background effects were computed (Table 10). They are almost infinitesimally small compared to the volume of the BMZ, ranging from 0.006% to 0.4%.

The fraction of the ambient flow passing over the BMZ that is entrained by the diffuser, and therefore the fraction of larvae that is entrained, was estimated (Table 10). For the brine discharges, it ranges from 1.7% to 6.4%.

Not all of the organisms that are entrained by the diffuser will die. The fraction of organisms passing over the diffuser that die is estimated to be less than 0.23%. As discussed, this is believed to be a very conservative estimate. Total incremental mortality was also estimated in Table 11.

The volumes entrained into the brine discharges are compared to that for the present baseline domestic wastewater discharge case (P1). They are much lower, ranging from 7 to 22%. This is mainly because the dilutions for the domestic discharges are much higher. Therefore, organism mortality for the brine discharges would also be expected to be about 7 to 22% of the baseline case.

LIST OF FIGURES

LIST OF TABLES

1. INTRODUCTION

1.1 Study Purpose

It is proposed to dispose of the brine concentrate resulting from reverse osmosis (RO) seawater desalination into Monterey Bay, California. The disposal will be through an existing outfall and diffuser usually used for domestic wastewater disposal. Previous analyses of the mixing characteristics and dilution of the effluent were made by Flow Science (2008), and updated in 2014 (Flow Science, 2014) to accommodate new flow scenarios. The 2014 analysis used the same procedures as the 2008 report although new research on the dynamics of dense jets has been reported since 2008 and reviews and testimony have raised new questions. In addition, water quality requirements for concentrate discharges around the world and the literature on the environmental impacts of brine discharges were reviewed in SCCWRP (2012), leading to the revision of the California Ocean Plan (SWRCB, 2016) to include brine discharges. These revisions include new requirements on concentrate disposal, in particular the definition of a brine mixing zone (BMZ) at whose boundary salinity increment limitations must be met and within which salinity must be estimated. New issues were also raised, particularly the effect of velocity shear and turbulence on the mortality of larvae and other organisms that are entrained into the high velocity diffuser jets. New flow scenarios consisting of various combinations of brine and treated domestic effluent have also been proposed, and new data on density stratification around the diffuser have been obtained. Finally, no detailed computations of the internal flow hydraulics of the diffuser have been made to address the variation of flow along the diffuser and its effect on dilution.

The purpose of this report is to analyze the internal hydraulics of the outfall and diffuser, to update the analyses of the dynamics and mixing of various discharge scenarios, and to address the new issues raised, particularly the effects of velocity shear and jet turbulence.

Specific tasks are:

- Compute outfall and diffuser internal hydraulics and flow distribution accounting for the effects of check valves;
- Recompute dilutions for various scenarios of flow and effluent density;
- For dense discharges, compute salinity within the BMZ and at its boundary;
- Estimate regions where salinity exceeds 2 ppt;
- For buoyant discharges, compute dilutions and plume behavior for the new oceanic density stratification data;
- Address shear and turbulence mortality;

- Discuss mitigation, i.e. modifications to the diffuser if improvements to mixing are indicated.

The ambient receiving water conditions and new data are discussed in Section 2.1, and the discharge scenarios are discussed in Sections 2.2 and 2.3 and summarized in Section 2.4. Details of the outfall and diffuser are presented in Section 3 and results of the hydraulics analyses are summarized. The calculation procedure is detailed in Appendix A.

1.2 California Ocean Plan

The 2015 California Ocean Plan (SWRCB, 2016, revised and effective January 28, 2016), contains new requirements to address brine discharges. The most relevant of these to the present report are contained in Section III.M.3, "Receiving Water Limitation for Salinity" which states that:

"Discharges shall not exceed a daily maximum of 2.0 parts per thousand (ppt) above natural background salinity measured no further than 100 meters (328 ft) horizontally from each discharge point. There is no vertical limit to this zone…

the Brine Mixing Zone is the area where salinity may exceed 2.0 parts per thousand above natural background salinity, or the concentration of salinity approved as part of an alternative receiving water limitation. The standard brine mixing zone shall not exceed 100 meters (328 feet) laterally from the points of discharge and throughout the water column…

The brine mixing zone is an allocated impact zone where there may be toxic effects on marine life due to elevated salinity…

For operational mortality related to discharges, the report shall estimate the area in which salinity exceeds 2.0 parts per thousand above natural background salinity or a facility-specific alternative receiving water limitation (see chapter III.M.3). The area in excess of the receiving water limitation for salinity shall be determined by modeling and confirmed with monitoring. The report shall use any acceptable approach approved by the regional water board for evaluating mortality that occurs due to shearing stress resulting from the facility's discharge, including any incremental increase in mortality resulting from a commingled discharge."

2. MODELING SCENARIOS

2.1 Environmental Conditions

The discharges are to be made through the existing Monterey Regional Water Pollution Control Agency (MRWPCA) wastewater outfall offshore of Marina, California, shown in Figure 1. The dynamics and mixing of the discharges depend on the receiving water density structure and ocean currents. The analyses presented here assume zero current speed, which is the worst-case condition in terms of dilution, so the main environmental parameter is the receiving water density structure. Particularly important is the density difference between the effluent and receiving water, and, for buoyant discharges, the density stratification over the water column.

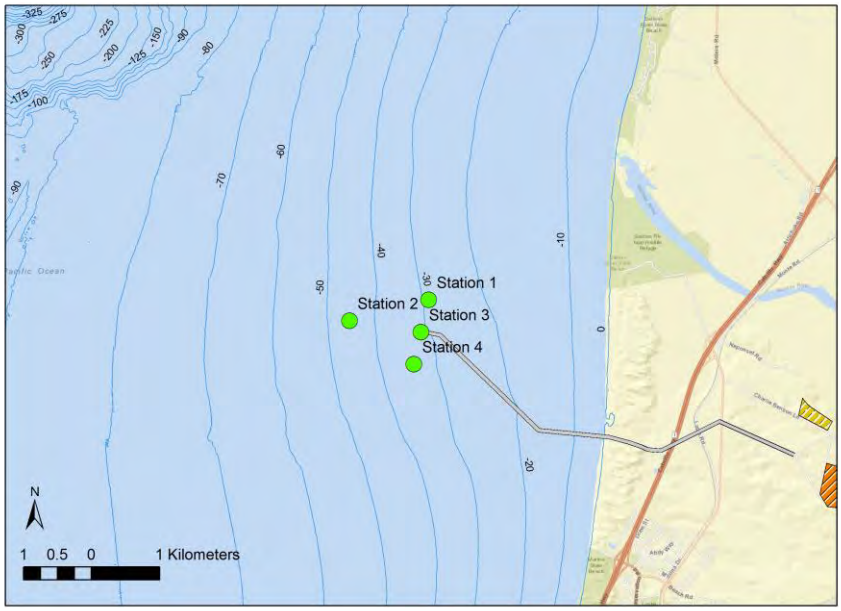

Figure 1. MRWPCA outfall near Marina, CA., and sampling locations for water column profiles. Bathymetry is in meters.

Monthly measurements of CTD (conductivity-temperature-depth) were made by Applied Marine Sciences (AMS, 2016) over the water column at the four locations shown in Figure 1. The objective of the monitoring was to gather data over a two-year period that reflected ocean conditions during this time period around the MRWPCA outfall. Monthly data were collected between February 2014 and December 2015.

Traditionally, three oceanic seasons have been defined in Monterey Bay: Upwelling (March-September), Oceanic (September-November), and Davidson (November-March). Therefore, the profiles were assessed with consideration given to these seasons, as well as over the entire sampling period.

It was found that there was little variation between the profiles taken at the four sites in any one day, so they were averaged together; they are plotted by season in Figure 2. The Upwelling season showed the most variable vertical structure in temperature and density. The Oceanic and Davidson seasons showed weak stratifications with essentially well-mixed temperature profiles with the oceanic season somewhat cooler than Davidson. Salinity was fairly uniform over depth so density was often controlled by temperature. The Upwelling season showed the strongest stratifications over the water column, and the profiles separate into two distinct groups with stratification for the other seasons being generally quite weak. Density differences over the water column ranged from zero (homogeneous) in December 2012 to 1.17 kg/m^3 in August 2014. For most of the profiles the density differences over the water column ranges from 0.11 to 0.65 kg/m^3.

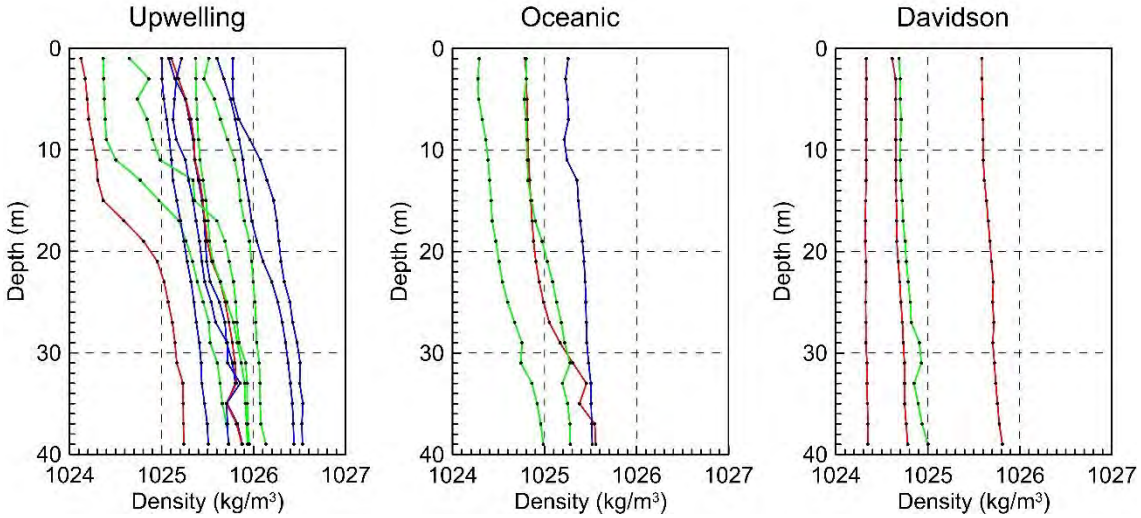

Figure 2. Seasonal density profiles at the sites shown in Figure 1.

The profiles within each season were then averaged to obtain representative profiles for the dilution simulations. The profiles are shown in Figure 3 and are tabulated in Appendix B.

Monthly variations of salinity near the depth of the diffuser (assumed to be the measurements around 27 to 29 m) are shown in Figure 4. The salinities vary seasonally, but little between the sites or the chosen depths. The bottom salinities and temperatures were averaged seasonally as summarized in Table 1.

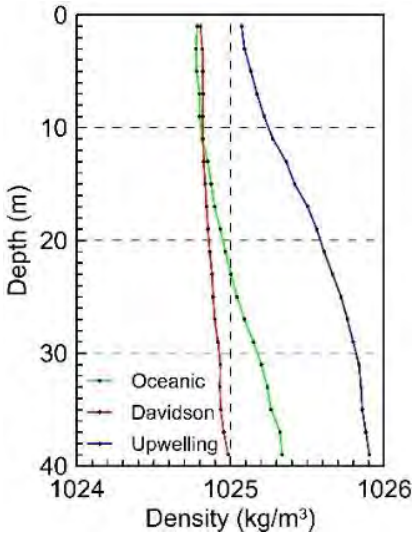

Figure 3. Seasonally averaged density profiles.

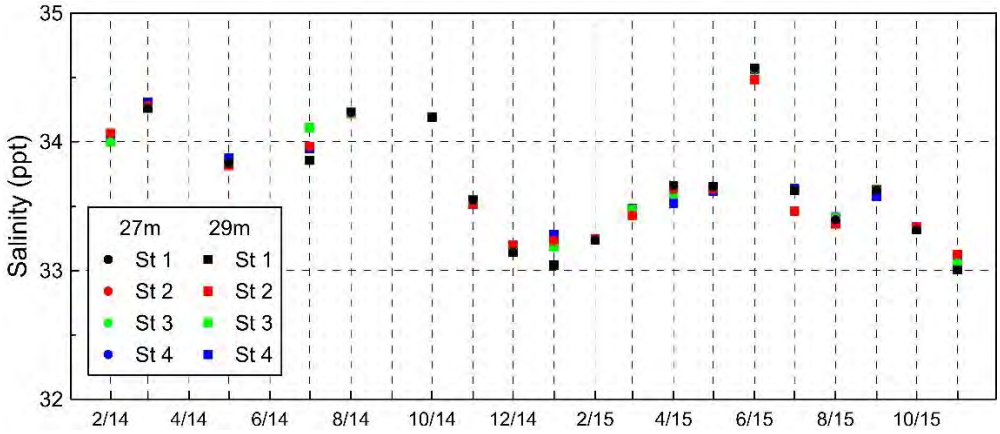

Figure 4. Monthly salinity variations at 27 and 29 m depths.

Table 1. Seasonal Average Properties at Diffuser Depth

Season	Temperature (°C)	Salinity (ppt)	Density (kg/m^3)
Davidson	14.46	33.34	1024.8
Upwelling	11.48	33.89	1025.8
Oceanic	13.68	33.57	1025.1

2.2 Discharge Scenarios Under Proposed Project

The Monterey Peninsula Water Supply Project (MPWSP) Desalination Plant would treat the source oceanic water at a 42 percent recovery rate to produce 9.5

mgd of desalinated product water. Approximately 14 mgd of brine would be generated, consisting of concentrates from the pretreatment and reverse osmosis (RO) processes as well as waste effluent produced during routine backwashing and operation and maintenance of the pretreatment filters. The brine generated in the desalination process would be discharged into Monterey Bay through the MRWPCA's existing ocean outfall. The outfall consists of an 11,260-foot-long pipeline terminating in a diffuser with 129 operational ports at a depth of approximately 100 feet. The outfall and diffuser and their internal hydraulics are discussed further in Section 3.

During certain times of the year, the brine would be blended with treated wastewater (when available) from the MRWPCA Regional Wastewater Treatment Plant, forming a combined discharge. Table 2 (Table 4.3-8 from the DEIR) shows the monthly projected brine flows from the MPWSP Desalination Plant and the average monthly wastewater flows from MRWPCA.

Table 2. Monthly Average Flows of Secondary Wastewater from the MRWPCS Treatment Plant (mgd) (1998–2012) and Estimated Brine Flows Under the MWPWSP

Months	Jan	Feb	Mar	Apr	May	Jun	Jul	Aug	Sept	Oct	Nov	Dec
Brine-Only	*13.98*	13.98	13.98	13.98	13.98	13.98	*13.98*	13.98	*13.98*	13.98	13.98	13.98
Treated Wastewater from MRWPCA	*19.78*	18.41	14.68	7.02	2.40	1.89	0.90	1.03	2.79	9.89	17.98	19.27
Combined Discharge (Brine+wastewater)	*33.76*	32.39	28.66	21.00	16.38	15.87	14.88	15.01	16.77	23.87	31.96	33.25

NOTE: Shaded cells represent the seasonal discharge scenarios used in the analysis of operational water quality impacts.

Numbers in *italics* represent the flow rates used in the modeling analysis of salinity (discussed in Impact 4.3-5), the results of which were used to analyze other constituents in the brine and combined discharges (discussed below in this impact analysis). In the case of the combined discharge, the modeling analysis also used low wastewater flow rates of 0.25, 0.5, 1, and 2 mgd and a moderate flow of 9 mgd.

SOURCES: MRWPCA, 2013; Trussell Technologies, 2015 in DEIR Appendix D4.

As shown in Table 2, the treated wastewater flow varies throughout the year, with the highest flows observed during the non-irrigation season (November through March) and the lowest flows during the irrigation season (April through October), when the treated wastewater is processed through the SVRP for tertiary treatment and distributed to irrigators through the Castroville Seawater Intrusion Project (CSIP).

During the irrigation season, on some days, all of the wastewater flows could be provided to irrigators, and only the project brine would be discharged into Monterey Bay through the outfall. The analysis presented in the DEIR assumed that the brine would be discharged without dilution during the entire irrigation season (dry months), reflected in scenario 2 in Table 3.

During the non-irrigation season (wet months), the analysis presented in the DEIR assumed that a combined discharge (i.e. brine blended with treated wastewater) would be released. For the combined discharge scenario, the data analysis accounted for different wastewater flows ranging from 19.78 mgd in the winter/Davidson season (when higher discharge flows are anticipated) to lower flows of 1 and 2 mgd (Table 3). Scenarios 3 through 6 reflect the proposed combined project discharges during the non-irrigation season as well as during the irrigation season when a low volume of secondary effluent is discharged.

Table 3. Proposed Project Discharge Scenarios

No.	Scenario	Discharge flows (mgd)	
		Secondary Effluent	Desal Brine
1	Baseline	19.78[a]	0
2	Desal only	0	13.98
3	Desal and low SE[b]	1	13.98
4	Desal with low SE	2	13.98
5	Desal with moderate SE	9	13.98
6	Desal with high SE	19.78	13.98

[a] All model scenarios involving high secondary effluent flows used for assessing impacts related to the proposed and variant project conditions use the maximum documented average wet season wastewater flow of 19.78 mgd.
[b] Secondary effluent

2.3 Discharge Scenarios Under Project Variant

Under the Project Variant, the MPWSP Desalination Plant would treat 15.5 mgd of source water at a 42 percent recovery rate. Approximately 8.99 mgd of brine would be generated, consisting of concentrates from the pretreatment and reverse osmosis (RO) processes as well as waste effluent produced during routine backwashing and operation and maintenance of the pretreatment filters. The brine generated in the desalination process would be discharged through the MRWPCA ocean outfall as with the Proposed Project (above).

The Project Variant would also include operation of the proposed Groundwater Replenishment Project (GWR) Project, which would involve RO treatment of a minimum of 3.9 mgd of source water to produce 3.2 mgd of product water and 0.73 mgd of effluent[1]. Operation of the Project Variant would result in discharge scenarios that would include brine from the MPWSP Desalination Plant,

[1] A minimum of 4,320 acre-feet per year (AFY) of source water would be treated to produce 3,500 AFY of product water. At the time of this analysis, the available data for the GWR Project, i.e., 0.73 mgd of GWR effluent flow was used for the modeling analysis (also see Flow Science, Inc., 2014).

and/or effluent from the proposed GWR project, and/or treated wastewater from the existing MRWPCA wastewater treatment plant. Depending on the operational scenario, the following discharges (also summarized in Table 4) would be released into Monterey Bay through the MRWPCA outfall:

Variant Scenario 1, Brine-only: 8.99 mgd of brine would be generated at the Desalination Plant and discharged alone through the MRWPCA outfall. This operating scenario would occur if the GWR Project comes on line after the MPWSP Desalination Plant, or the GWR Project periodically shuts down.

Variant Scenarios 2 through 5, Brine-with-Wastewater: 8.99 mgd of brine would be discharged with varying volumes of treated wastewater from the MRWPCA Regional Wastewater Treatment Plant. This operating scenario would occur when treated wastewater is available and if the GWR Project comes on line after the MPWSP Desalination Plant, or the GWR Project periodically shuts down.

(Previously modeled, no update needed) GWR-only discharge: 0.94 v of effluent generated under the MRWPCA-proposed GWR Project would be discharged alone through the MRWPCA outfall. This operating scenario would occur if the GWR Project comes on line before the MPWSP Desalination Plant, or the MPWSP Desalination Plant periodically shuts down.

Variant Scenario 6, Blended discharge: 8.99 mgd of brine generated from the MPWSP Desalination Plant would be blended with 0.94 mgd of GWR-effluent. This operating scenario would typically occur in the irrigation season.

Variant Scenarios 7 through 10, Combined discharge: The blended discharge (brine and GWR effluent) would be combined with varying volumes of treated wastewater from the MRWPCA Regional Wastewater Treatment Plant. This operating scenario would typically occur in the non-irrigation season.

Not Modeled, GWR-with-Wastewater: 0.94 mgd of GWR-effluent would be discharged with varying volumes of treated wastewater from the MRWPCA Regional Wastewater Treatment Plant without brine generated from the MPWSP Desalination Plant. This operating scenario would occur when treated wastewater is available and if the GWR Project comes on line before the MPWSP Desalination Plant, or the MPWSP Desalination Plant periodically shuts down. These scenarios have been modeled and impacts assessed and documented in the Final EIR for the Pure Water Monterey GWR Project (MPWPCA, 2015).

Table 4. Variant Project Discharge Scenarios

No	Scenario	Discharge flows (mgd)		
		Secondary Effluent	Desal Brine	GWR
1	Desal only	0	8.99	0
2	Desal and low (1) SE	1	8.99	0
3	Desal and low (2) SE	2	8.99	0
4	Desal and moderate SE	5.8 (Davidson)	8.99	0
5	Desal and high SE	19.78	8.99	0
6	Desal and GWR	0	8.99	0.94
7	Desal and GWR and low (1) SE	1	8.99	0.94
8	Desal and GWR and low (2) SE	3	8.99	0.94
9	Desal and moderate SE and GWR	5.3 (Upwelling)	8.99	0.94
10	Desal and high SE and GWR	15.92	8.99	0.94

Notes:

[a] All model scenarios involving high secondary effluent flows used for assessing impacts related to the proposed and variant project conditions use the maximum documented average wet season wastewater flow of 19.78 mgd.

2.4 Updated Model Scenarios

The assumed effluent characteristics for the three seasonal scenarios are summarized in Table 5.

Table 5. Assumed Effluent Characteristics

Season	Brine[1]		Secondary Effluent[1]		GWR	
	Salinity (PPT)	Temp (°C)	Salinity (PPT)	Temp (°C)	Salinity [2] (PPT)	Temp[1] (°C)
Upwelling	58.23	9.9	0.8	24	5.8	24.4
Davidson	57.40	11.6	0.8	20	5.8	20.2
Oceanic	57.64	11.1	0.9	24	5.8	24.4

[1]FlowScience (2014), Table C3 and C6 (p.C-7 and C-17), Appendix C.

[2]Pure Water Monterey Groundwater Replenishment Project Consolidated FEIR (2016):
"The discharge of reverse osmosis concentrate would not involve high salinities because the concentrate would be far less saline than ambient ocean water (5,800 mg/L of TDS compared to 33,000 to 34,000 mg/L). The secondary effluent (approximately 1,000 mg/L of TDS) and GWR reverse osmosis concentrate (approximately 5,000 mg/L of TDS) are relatively light and would rise when discharged."
Note: Salinity value of 4 PPT for GWR effluent estimated in Flow Science (2014).

Using the discharge scenarios in Table 3 for the Proposed Project and in Table 4 for the Project Variant, previous model analyses will be updated as follows:

Revise the near-field brine discharge modeling by adjusting the number of open ports (129 versus 120 used prior), the height of the ports off the ocean floor (4 feet versus 3.5 feet used prior), and flow scenarios (Table 2 for the Project and Table 3 for the Variant).

Using the revised modeling for each scenario, compute dilution ratios, calculate the volume of ocean water that exceeds 2 ppt above ambient, plot the gradient of salinity between the port and the edge of the Zone of Initial Dilution ZID, calculate the eddy size and velocity of the plume and determine marine losses due to shear stress, if any. Also calculate the salinity beyond the ZID but within the regulatory mixing zone (100 m from the port).

Combining the assumed environmental conditions from Table 1, the flows from Tables 3 and 4, and the assumed effluent conditions from Table 5, we arrive at 16 possible flow scenarios. Their conditions are summarized in Table 6. The Proposed Project scenarios are labeled P1 though P6 and the Project Variant scenarios are Labeled V1 through V10.

Table 6. Modeled Discharge Scenarios

Case No.	Season	Background			Brine			Secondary effluent			GWR			Combined discharge		
		Temp. (°C)	Salinity (ppt)	Density (kg/m^3)	Flow (mgd)	Temp. (°C)	Salinity (ppt)	Flow (mgd)	Temp. (°C)	Salinity (ppt)	Flow (mgd)	Temp. (°C)	Salinity (ppt)	Flow (mgd)	Salinity (ppt)	Density (kg/m^3)
P1	Baseline	-	-	-	-	-	-	19.78	20.0	0.8	0	20.0	5.8	19.78	0.80	998.8
P2	Upwelling	11.48	33.89	1025.8	13.98	9.9	58.23	0	24.0	0.8	0	24.4	5.8	13.98	58.23	1045.2
P3	Davidson	14.46	33.34	1024.8	13.98	11.6	57.40	1.00	20.0	0.8	0	20.2	5.8	14.98	53.62	1041.2
P4	Davidson	14.46	33.34	1024.8	13.98	11.6	57.40	2.00	20.0	0.8	0	20.2	5.8	15.98	50.32	1038.5
P5	Davidson	14.46	33.34	1024.8	13.98	11.6	57.40	9.00	20.0	0.8	0	20.2	5.8	22.98	35.23	1026.4
P6	Davidson	14.46	33.34	1024.8	13.98	11.6	57.40	19.78	20.0	0.8	0	20.2	5.8	33.76	24.24	1017.6
V1	Upwelling	11.48	33.89	1025.8	8.99	9.9	58.23	0	24.0	0.8	0	24.4	5.8	8.99	58.23	1045.2
V2	Upwelling	11.48	33.89	1025.8	8.99	9.9	58.23	1.00	24.0	0.8	0	24.4	5.8	9.99	52.48	1040.5
V3	Upwelling	11.48	33.89	1025.8	8.99	9.9	58.23	2.00	24.0	0.8	0	24.4	5.8	10.99	47.78	1036.6
V4	Davidson	14.46	33.34	1024.8	8.99	11.6	57.40	5.80	20.0	0.8	0	20.2	5.8	14.79	35.20	1026.4
V5	Upwelling	11.48	33.89	1025.8	8.99	9.9	58.23	19.78	24.0	0.8	0	24.4	5.8	28.77	18.75	1012.7
V6	Upwelling	11.48	33.89	1025.8	8.99	9.9	58.23	0	24.0	0.8	0.94	24.4	5.8	9.93	53.27	1041.1
V7	Davidson	14.46	33.34	1024.8	8.99	11.6	57.40	1.00	20.0	0.8	0.94	20.2	5.8	10.93	47.78	1036.5
V8	Davidson	14.46	33.34	1024.8	8.99	11.6	57.40	3.00	20.0	0.8	0.94	20.2	5.8	12.93	40.52	1030.6
V9	Upwelling	11.48	33.89	1025.8	8.99	9.9	58.23	5.30	24.0	0.8	0.94	24.4	5.8	15.23	35.01	1026.1
V10	Davidson	14.46	33.34	1024.8	8.99	11.6	57.40	15.92	20.0	0.8	0.94	20.2	5.8	25.85	20.67	1014.7

3. OUTFALL HYDRAULICS

The Monterey Regional Water Pollution Control Agency (MRWPCA) outfall at Marina, shown in Figure 5, conveys the effluent to the Pacific Ocean to a depth of about 100 ft below Mean Sea Level (MSL). The ocean segment extends a distance of 9,892 ft from the Beach Junction Structure (BJS). Beyond this there is a diffuser section 1,406 ft long. The outfall pipe consists of a 60-inch internal diameter (ID) reinforced concrete pipe (RCP), and the diffuser consists of 480 ft of 60-inch RCP with a single taper to 840 ft of 48-inch ID. The diffuser has 171 ports of two-inch diameter: 65 in the 60-inch section and 106 in the 48-inch section. The ports discharge horizontally alternately from both sides of the diffuser at a spacing of 16 ft on each side except for one port in the taper section that discharges vertically for air release. The 42 ports closest to shore are presently closed, so there are 129 open ports distributed over a length of approximately 1024 ft. The 129 open ports are fitted with four inch Tideflex "duckbill" check valves (the four inch refers to the flange size not the valve opening). The valves open as the flow through them increases so the cross-sectional area is variable. The end gate has an opening at the bottom about two inches high. The effect of the valves on the flow distribution in the diffuser is discussed in Appendix A.

Figure 5. The MRWPCA outfall

The diffuser section sits on rock ballast as shown in Figure 6. The ports are approximately six inches above the rock ballast and nominally 54 inches above the sea bed, although this varies. For the dilution calculations, they are assumed to be 4 ft above the bed. The diffuser is laid on a slope of about 0.011 and the depths of the open ports range from about 98 to 110 ft below MSL.

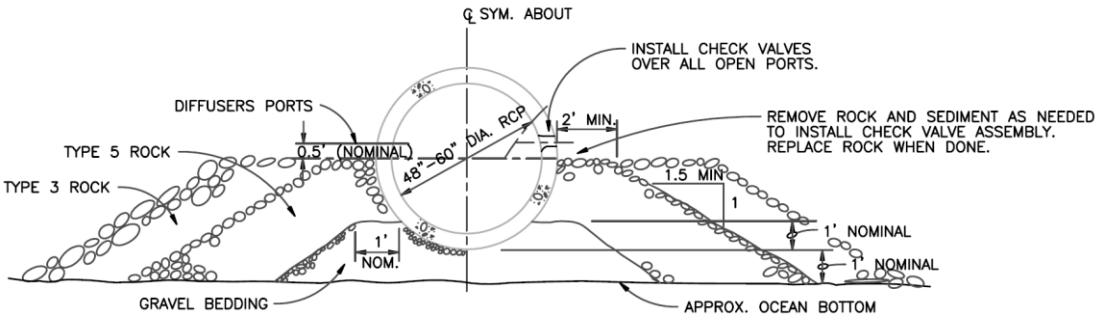

Figure 6. Typical diffuser cross section

The procedure for analyzing the internal hydraulics of the outfall and diffuser is discussed in Appendix A. Using these procedures, the head losses and the flow distribution between the ports and the end gate port were computed for the various flow scenarios of Table 6. Some typical distributions of flow among the ports, for scenarios P1 (19.78 mgd of secondary effluent), P2 (13.98 mgd of pure brine), and P6 (33.76 mgd of brine and secondary effluent) are shown in Figure 7.

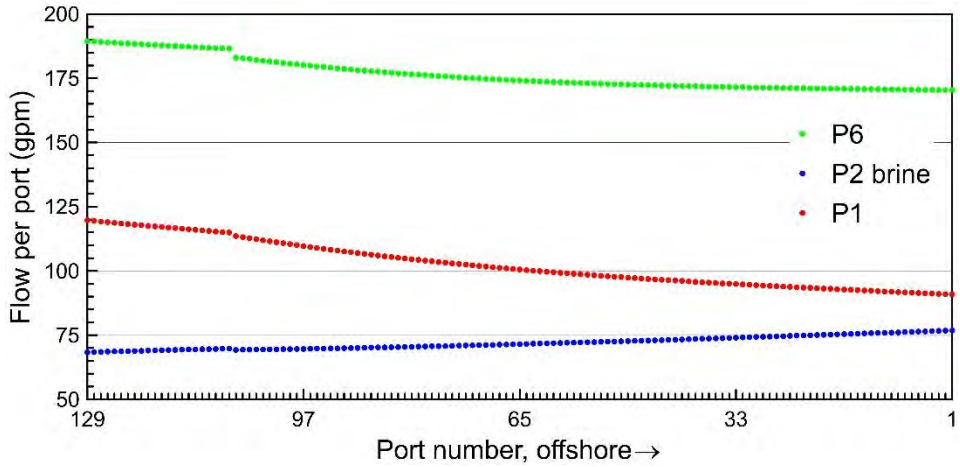

Figure 7. Typical port flow distributions.

For the pure brine discharge P2 (density greater than seawater) the flow per port increases in the offshore direction because of the density head. For the buoyant discharges P1 and P6 (less dense than seawater) the flow decreases in the offshore direction. The port discharges vary by about ±7% from the average, and about 5% of the flow exits from the opening in the end gate. These flow variations are accounted for in the dilution simulations, and the worst cases for dilution are chosen.

4. DENSE DISCHARGE DILUTION

4.1 Introduction

Discharges that are more dense than the receiving seawater result in a sinking plume that impacts the sea floor at some distance from the nozzle as shown in Figure 8. The jet, because of its high exit velocity, entrains seawater that mixes with and dilutes the effluent.

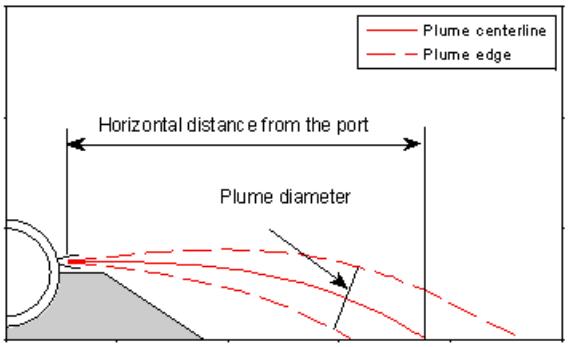

Figure 8. Horizontal dense jet dynamics (DEIR, Appendix D2).

Three-dimensional laser-induced fluorescence (3DLIF) images of a horizontal negatively buoyant jet similar to those considered here are shown in Figure 9. The images are obtained by scanning a laser sheet horizontally thought the flow to which a small amount of fluorescent dye has been added. The fluoresced light is captured and converted to tracer concentrations and dilution and imaged by computer graphics techniques as described in Tian and Roberts (2003). The left image shows the outer surface of the jet in gray scale and the right image shows the outer surface as semi-transparent with tracer concentrations in false color in a vertical plane through the jet centerline.

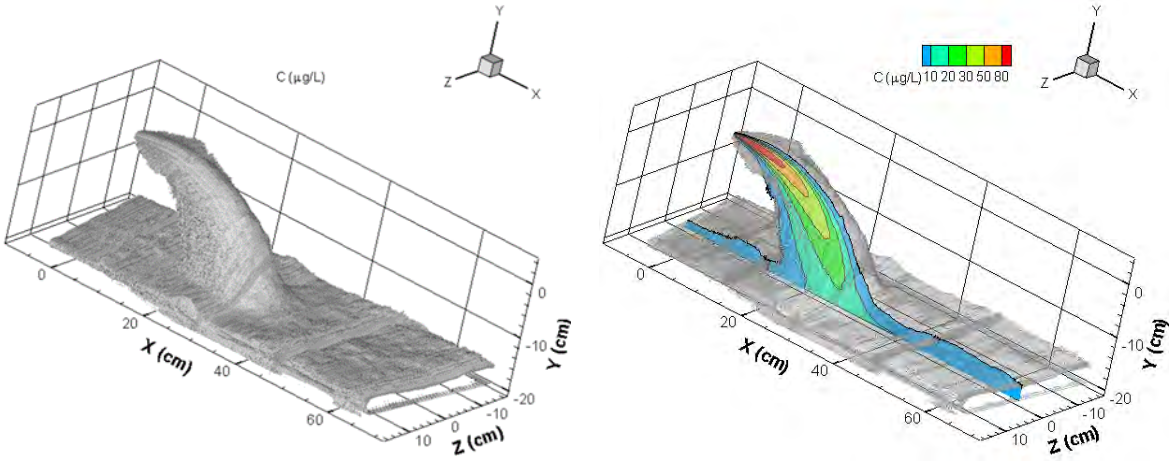

Figure 9. 3DLIF images of horizontal dense jet (Nemlioglu and Roberts, 2006).

It can be seen that high tracer concentrations (i.e. salinity) are confined to a relatively small volume near the nozzle and attenuate rapidly with distance from the nozzle. The highest salinity on the floor occurs where the jet centerline impacts it, and it is the dilution and salinity at this point that is computed here.

In the Flow Science (2014) report, they analyze this situation using a semi-empirical method and also the mathematical model UM3 in the US EPA model suite Visual Plumes. In the semi-empirical method, the jet trajectory and impact point are predicted by an analysis due to Kikkert et al. (2007) and dilution was then predicted by assuming it to occur from jet-induced entrainment. Although the Kikkert analysis can be applied, it was derived primarily for upwardly-inclined dense jets rather than horizontal, as occur here, and the dilution analysis neglects any effects of buoyancy on entrainment. Furthermore, the Flow Science report considers the centerline dilution predictions of the entrainment model UM3 to be unreliable due to a study by Palomar at al. (2012a, 2012b) which concluded that UM3 (and other entrainment models) underestimated impact dilutions by 50-65%. They therefore used UM3 *average* dilutions as estimates of *centerline* dilutions. The observations of Palomar et al., however, only applied to jets inclined upwards at 30° to 60° to the horizontal, where mixing is greater due to gravitational instabilities. For small fractional density differences, the dynamics of horizontal dense jets are the same as for positively buoyant jets (with a change in the sign of the density difference). Therefore, a simpler semi-empirical analysis can be applied, and UM3, which is well-tested and validated for such situations, is also applicable. The new analysis and application of UM3 are described below.

For the jet situation shown in Figures 8 and 9 it can be shown that the centerline dilution S_m at any vertical distance z from the nozzle is given by (Roberts et al. 2010):

$$\frac{S_m}{F_j} = f\left(\frac{z}{dF_j}\right) \tag{1}$$

where F_j is the densimetric Froude number of the jet:

$$F_j = \frac{u_j}{\sqrt{g_o' d}} \tag{2}$$

u_j is the jet velocity, $g_o' = g(\rho_a - \rho_o)/\rho_o$ is the modified acceleration due to gravity, g is the acceleration due to gravity, ρ_a and ρ_o are the ambient and effluent densities, respectively, and d the (round) nozzle diameter. Experimental measurements of the centerline dilutions plotted according to Eq. 1 are shown in Figure 10.

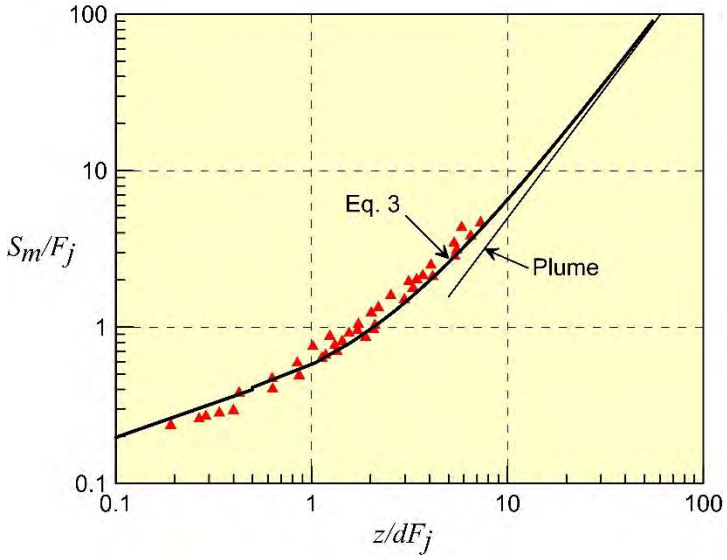

Figure 10. Centerline dilution of a horizontal buoyant jet into a stationary homogeneous environment (Roberts et al. 2010).

A fit to these data for $z/dF_j > 0.5$ has been suggested by Cederwall (1968):

$$\frac{S_m}{F_j} = 0.54\left(0.66 + 0.38\frac{z}{dF_j}\right)^{5/3} \tag{3}$$

which is plotted on Figure 10. This equation is used to predict dilutions below.

The dilution and trajectories of the jets can also be predicted by UM3. UM3 is a Lagrangian entrainment model described in Frick (2003, 2004).

4.2 Results

The following procedure was followed to determine the dilutions for dense discharges. First the internal hydraulics program (Section 3) was run for each case summarized in Table 6 to determine the flow distribution between the ports. Because the flow varies between the ports and because the effective port diameter varies with flow rate, it is not immediately obvious where along the diffuser the lowest dilution will occur. Therefore, dilutions were computed for the innermost and outermost ports. Depending on flow and density, the innermost ports would sometimes discharge the lowest flow, and sometimes the highest. The conditions resulting in lowest dilutions were chosen; sometimes this would occur at the innermost port and sometimes the outermost.

A typical jet trajectory output from UM3 (for the pure brine case, P2) is shown in Figure 11. For this case, the jet centerline impacts the seabed about 10 ft from the nozzle and the jet diameter is about 5 ft. Similar simulations were run for all dense scenarios, and the results, using the Cederwall formula and UM3, are summarized in Table 7.

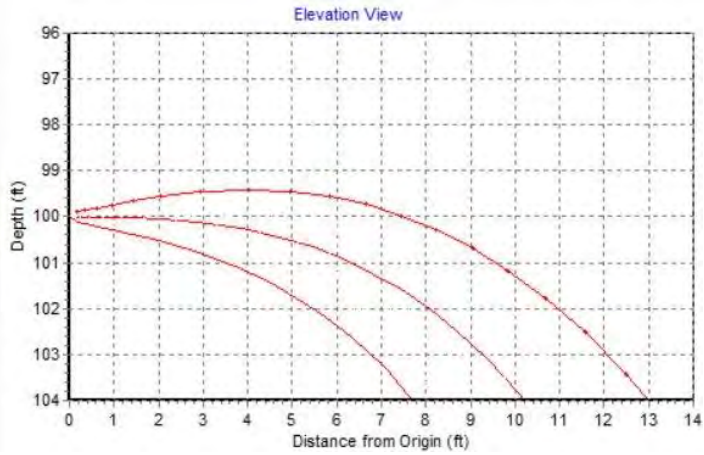

Figure 11. Typical graphics output of jet trajectory from UM3: Pure brine case, P2.

It is remarkable how close the dilution predictions of UM3 and Cederwall are. Cederwall's are generally more conservative, so these values are adopted. Jet impact distances from UM3 are also shown in Table 7. Jet diameters are generally much less than the port spacing of 16 ft, so no merging is expected before bottom impaction. The results are comparable to the Flow Science semi-empirical method.

The worst case, as expected, is the pure brine case, P2. For this case, the minimum centerline dilution is 15.5 and the salinity increment is 1.6 ppt, well within the BMZ limit of 2 ppt. The distance up to the impact point can be interpreted as the Zone of Initial Dilution (ZID). In all cases, the salinity limit is met within the ZID, whose length ranges from about 9 ft for scenario V1 up to 42 ft for scenario V9, where the density difference is much less and the jet trajectory is much flatter.

The jets will continue to dilute and will ultimately merge beyond the ZID. The increase in dilution up to the edge of the BMZ is difficult to estimate as there are no experiments available for these horizontal dense jet flows. Some guidance can be obtained from experiments on buoyant jets and inclined dense jets, however. Roberts et al. (1997) estimates a dilution increase of about 60% from the impact point to the end of the near field for single (non-merging) 60° inclined jets. For merged jets or plumes the increase in dilution is less; Abessi and Roberts (2014) reported a dilution increase of about 22% from impact point to the end of the near field. This is in keeping with the differences in dilution between non-merged and merged positively buoyant jets impacting water surfaces reported in Tian et al. (2004). The spacing between the individual jets on each side of the diffuser is 16 ft therefore it is conservatively assumed that they will merge within the BMZ and the increase in dilution from the impact point to the BMZ is 20%. This increase is used to predict the BMZ dilutions in Table 7.

Table 7. Summary of Dilution Simulations for Dense Effluent Scenarios

Case No.	Background conditions		Effluent conditions		Port conditions						Cederwall formula			UM3		Cederwall at BMZ	
												Salinity					
	Salinity (ppt)	Density (kg/m^3)	Salinity (ppt)	Density (kg/m^3)	Flow (gpm)	Diam. (in)	Height (ft)	Velocity (ft/s)	Froude no.	z_o/dF	Dilution	At impact (ppt)	Incre-ment (ppt)	Dilution	Impact distance (ft)	Dilution	Salinity incre-ment-(ppt)
P1	-	-	0.80	998.8	-	-	-	-	-	-	-	-	-	-	-	-	-
P2	33.89	1025.8	58.23	1045.2	76.3	1.87	4.0	8.9	29.0	0.89	15.6	35.45	1.56	16.3	10.3	18.7	1.30
P3	33.34	1024.8	53.62	1041.2	75.0	1.86	4.0	8.9	31.4	0.82	16.2	34.60	1.25	16.9	10.7	19.4	1.04
P4	33.34	1024.8	50.32	1038.5	80.8	1.89	4.0	9.2	35.5	0.72	17.0	34.34	1.00	17.8	11.8	20.5	0.83
P5	33.34	1024.8	35.23	1026.4	117.8	2.07	4.0	11.2	120.3	0.19	38.7	33.39	0.05	35.3	29.0	46.5	0.04
P6	33.34	1024.8	24.24	1017.6	188.5	2.28	4.0	14.8	71.5	-	-	-	-	-	-	-	-
V1	33.89	1025.8	58.23	1045.2	50.8	1.67	4.0	7.4	25.6	1.12	15.9	35.42	1.53	16.3	8.7	19.0	1.28
V2	33.89	1025.8	52.48	1040.5	54.3	1.70	4.0	7.7	30.1	0.94	16.7	35.00	1.11	17.4	9.8	20.0	0.93
V3	33.89	1025.8	47.78	1036.6	54.6	1.71	4.0	7.6	34.7	0.81	17.7	34.67	0.78	18.5	10.9	21.3	0.65
V4	33.34	1024.8	35.20	1026.4	77.9	1.88	4.0	9.0	102.0	0.25	34.5	33.40	0.05	32.5	24.0	41.4	0.04
V5	33.89	1025.8	18.75	1012.7	160.8	2.21	4.0	13.5	48.9	-	-	-	-	-	-	-	-
V6	33.89	1025.8	53.27	1041.1	54.3	1.70	4.0	7.7	29.5	0.96	16.6	35.06	1.17	17.2	9.7	19.9	0.98
V7	33.34	1024.8	47.78	1036.5	58.3	1.74	4.0	7.9	34.2	0.81	17.4	34.17	0.83	18.2	10.9	20.9	0.69
V8	33.34	1024.8	40.52	1030.6	66.5	1.80	4.0	8.4	50.6	0.53	21.3	33.68	0.34	22.1	14.7	25.5	0.28
V9	33.89	1025.8	35.01	1026.1	77.8	1.88	4.0	9.0	260.5	0.10	77.1	33.90	0.01	55.4	42.1	92.5	0.01
V10	33.34	1024.8	20.67	1014.7	143.3	2.16	4.0	12.6	52.6	-	-	-	-	-	-	-	-

Finally, note that the computed salinities occur only along the seabed. Salinities decrease with height and will only be above ambient within the spreading layer on the bottom. For most of the water column, incremental salinities will be much less than the values in Table 7.

4.3 Other Considerations

The increase in dilution beyond the impact point, or ZID, above is the increase in dilution up to the end of near field, defined as (Abessi and Roberts, 2014) the point where the turbulence induced by the discharge collapses under the influence of its self-induced density stratification. Again, there are no direct experiments to estimate this distance for this horizontal flow case, but Abessi and Roberts (2014) estimate the ratio of the near field length to the impact distance to be about 3:1. The impact distances in Table 7 range from about 9 to 42 ft, so, assuming the ratio of 3:1 to apply here, the end of the near field will always be within the BMZ distance of 100 m (328 ft). The assumption that dilution stops at the end of the near field is a conservative one as further dilution will occur due wave effects and entrainment as the gravity current flows down the bottom slope.

The dilution calculations assume the discharges to be from round nozzles whose area is the same as the effective opening of the check valves. There are no models to predict the dilution from elliptically-shaped check valves but experiments (Lee and Tang, 1999) show that the centerline dilutions from elliptical nozzles are greater than from equivalent round nozzles due to the larger surface area available for entrainment and that the dilutions asymptotically approach those of equivalent round nozzles at about 12 equivalent jet diameters from the nozzle.

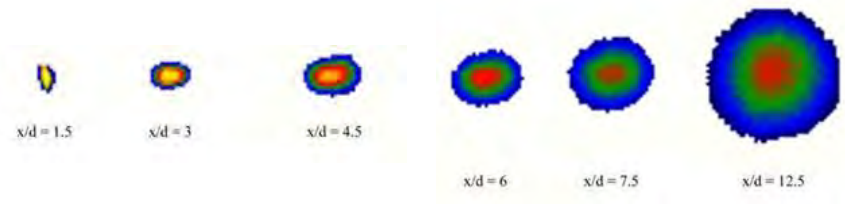

Figure 12. Cross sections of a jet from a check valve illustrating the transition from elliptical to round shapes. From Lee and Tang (1999).

Mixing of horizontal dense jets can also be affected by proximity to the local boundary which may cause a Coanda attachment. Some experiments on this phenomenon have been reported by Shao and Law (2011); a figure from their paper is shown in Figure 12. They find that the flow transitions to a wall-dense-jet with momentum continuing to play a role in mixing. They investigated Coanda attachment of the jet to the lower boundary and found that none occurred for a

parameter which they defined as: $z_o/l_M > 0.12$. This parameter is essentially the same as z_o/dF shown in Table 7. Only case V9 is close to this value and the dilutions for this cases are very high. It is therefore concluded that Coanda attachment will not have any effect on the dynamics or mixing of the brine jets. And furthermore, because of the strong mixing and entrainment in the wall jet region, it is expected that the additional dilution beyond the impingement point will be actually much greater than the 20% assumed above.

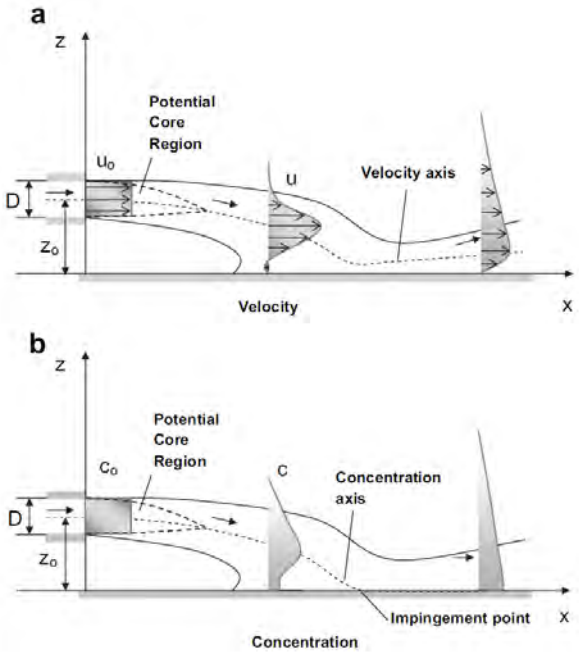

Figure 13. Dense jet impacting a local boundary. From Shao and Law (2011).

5. BUOYANT DISCHARGE DILUTION

5.1 Introduction

Positively buoyant (or just buoyant) discharges, i.e. that have densities less than the receiving seawater, require different procedures than for negatively buoyant ones. Inspection of Table 6 shows there are only four positively buoyant scenarios; P1, the baseline with pure secondary effluent, P6, high volumes of brine and secondary effluent, and V5 and V10, Project Variants with moderate brine volumes and high secondary effluent and GWR volumes. Positively buoyant effluents rise in the water column and are either trapped by the ambient density stratification if it is strong enough, or reach the water surface if it is weak. A laboratory photograph of a buoyant discharge from a multiport diffuser into a stationary stratified environment is shown in Figure 13.

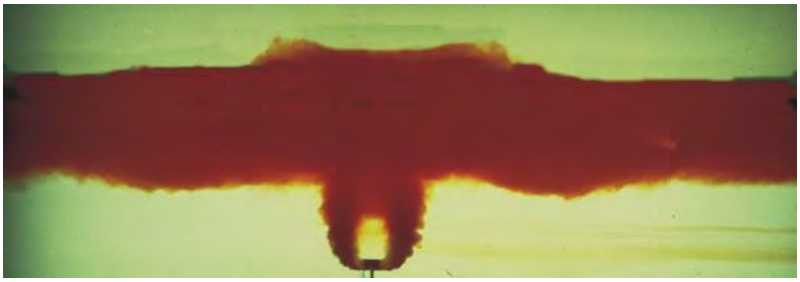

Figure 14. Trapped buoyant plume from multiport diffuser in stratified environment, from Roberts et al. (1989).

The plume dynamics are simulated with two models in Visual Plumes: UM3 and NRFIELD. UM3 is an entrainment model that was previously described. NRFIELD is based on the experiments on multiport diffusers discharging from two sides described in Roberts et al. (1989) and subsequently updated with the new experimental data of Tian et al. (2004) and others. NRFIELD is specifically designed for conditions typical of very buoyant discharges of domestic effluent from multiport diffusers into stratified oceanic waters so is judged most appropriate here. It also includes the lateral spreading after the terminal rise height and subsequent turbulent collapse at the end of the near field. The primary outputs from NRFIELD are the minimum (centerline) dilution, the plume rise height, and wastefield thickness at the end of the near field.

The following procedure was used for the dilution simulations. The internal hydraulics program, Section 3, was first run for each of the three scenarios. The average port diameter and flows were then obtained. UM3 and NRFIELD were then run for the chosen flow and ambient combination scenarios summarized in Table 6: P1 with Upwelling, Davidson, and Oceanic conditions; P6 with Davidson, and V5 with Upwelling. The seasonal average density stratifications that were

discussed in Section 2.1 and plotted in Figure 3 were used and zero current speed was assumed. UM3 assumes the discharges are from one side so the usual assumption was used that the diffuser consists of 129 ports spaced 8 ft apart. NRFIELD assumes the correct configuration of ports on either side spaced 16 ft apart; the correction is made internally in Visual Plumes.

5.2 Results

The results are summarized in Table 8 and some graphical jet trajectories from UM3 are shown in Figure 14. For UM3 the average dilutions at the terminal rise height are given along with the centerline rise heights, for NRFIELD the near field (minimum) dilution is given along with the height of the near field (centerline) dilution and the height to the top of the spreading wastefield layer.

Table 8. Summary of Dilution Simulations for Buoyant Effluent Scenarios

No.	Flow rate (mgd)	Effluent density (kg/m^3)	Port diam. (in)	Ocean condition	UM3 simulations		NRFIELD simulations		
					Average dilution	Rise height (center-line) (ft)	Minimum dilution	Rise height (center line) (ft)	Rise height (top) (ft)
P1	19.78	998.8	2.00	Upwelling	191	58	186	59	42
P1	19.78	998.8	2.00	Davidson	327	100 (surface)	351	100	100
P1	19.78	998.8	2.00	Oceanic	240	82	239	50	72
P6	33.76	1017.6	2.25	Davidson	154	86	163	86	89
V5	28.77	1012.7	2.18	Upwelling	122	47	105	41	43
V10	25.85	1014.7	2.13	Davidson	195	100 (Surface)	221	100	100

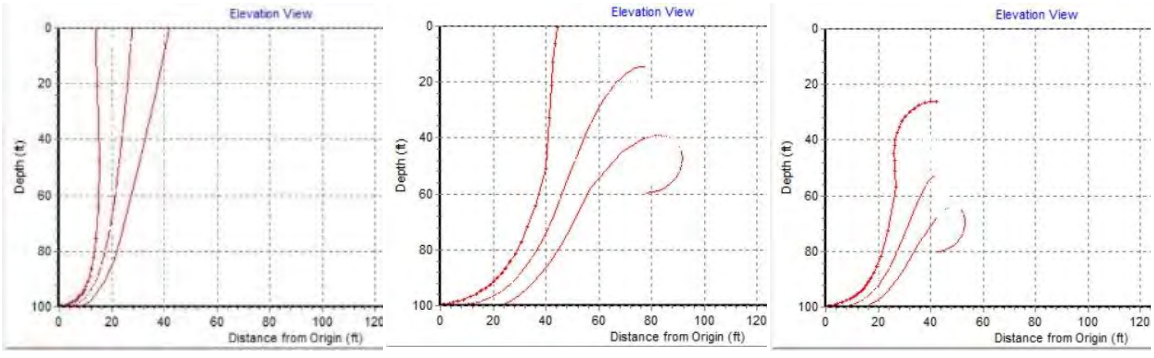

a) P1 Davidson **b) P6 Davidson** **c) V5 Upwelling**

Figure 15. Graphics outputs from UM3 simulations.

It can be seen that the *average* dilution predicted by UM3 is very close to *minimum* (centerline) dilution predicted by NRFIELD. Similar observations were

made by Isaacson et al. (1983) in connection with physical model studies on the San Francisco outfall. The reason is apparently that the increase in mixing and dilution in the transition from vertical to horizontal flow and merging of the plumes from both sides, neither of which are incorporated into UM3, are accounted for in the ratio of average to minimum dilutions. Therefore, we use the average dilution predicted by UM3 but interpret it as the minimum centerline dilution. Similar observations are reported in model comparisons by Frick and Roberts (2016). The near field dilution is synonymous with the initial dilution in the ZID as defined in the California Ocean Plan.

Dilutions are generally high: The lowest is 105 for scenario V5 which was run with strong (Upwelling) stratification. The highest dilution was 351 for scenario P1 (pure secondary effluent) with weak (Davidson) stratification which resulted in a surfacing plume. Generally speaking, strong stratification results in lower dilutions and reduced rise height, and weak stratification result in higher dilutions and increased rise height. All of the scenarios resulted in submerged plumes except for case P1 with Davidson conditions.

Note that all the simulations were run for zero current, as specified in the Ocean Plan. More realistic simulations with currents would predict higher dilutions and deeper submergences.

The lower density difference and therefore relatively greater influence of source momentum flux results in flatter jet trajectories, as seen in Figure 14ab, cases P6 and V5.

6. SHEAR AND TURBULENCE EFFECTS

6.1 Introduction

The 2015 California Ocean Plan contains the following requirement for mitigation of marine life or habitat lost due to a desalination facility:

> *"For operational mortality related to discharges, the report shall estimate the area in which salinity exceeds 2.0 parts per thousand above natural background salinity or a facility-specific alternative receiving water limitation (see chapter III.M.3). The area in excess of the receiving water limitation for salinity shall be determined by modeling and confirmed with monitoring. The report shall use any acceptable approach approved by the regional water board for evaluating mortality that occurs due to shearing stress resulting from the facility's discharge, including any incremental increase in mortality resulting from a commingled discharge."*

The purpose of this section is to evaluate mortality due to the discharge. In particular, it has been suggested that planktonic organisms entrained into the high velocity turbulent jets could be subject to injury, possibly mortality, due to the effects of turbulence and shear. This is difficult to estimate, so only approximate orders of magnitude can be made. Somewhat similar concerns arise due to entrainment into water intakes, for example Tenera (2014), although the considerations for jets are different and somewhat more complex.

Experimental evidence suggests that the main turbulence effect is caused by small-scale eddies, known as the Kolmogorov scales, and that most damage may occur when they are comparable to the size of the organisms. These small eddies subject the organism to high strain rates and viscous shear stress that may cause injury or death whereas larger eddies mainly translate the organisms without causing significant shear. The effects vary by organism, and a number of studies on the effects of flow and turbulence on marine and freshwater organisms have been reported. They are summarized in Appendix C.

Most relevant here are the studies of Rehmann et al. (2003) and Jessop (2007). Rehmann et al. performed laboratory experiments in which zebra mussel veligers were subject to controlled turbulence in beakers. The turbulence intensity was such that the Kolmogorov scale, $L_k \sim 0.1$ mm. They found that mortality increased sharply to about 65% when the size of the larvae was about 90% of the Kolmogorov scale. Jessop (2007) measured survival rates in a highly turbulent tidal channel with $0.06 < L_k < 0.25$ mm. Survival rates varied with species; thin-shelled veligers showed significant mortality of 45% to 64%, but some taxa showed no mortality.

These and other results are difficult to translate to jet turbulence for a number of reasons. In the laboratory experiments, the organisms were subject to fairly homogeneous turbulence for long periods: 24 hours. In the field experiment the turbulence was variable during the organisms' transit through the channel. The duration of exposure to high turbulence is unknown but was probably a few minutes and the variation of conditions during transit are also unknown.

In contrast, the turbulence in jets is not homogeneous: it varies along the centerline and also laterally across the jet. Kolmogorov scales are smallest near the nozzle and increase along the trajectory; they are shortest on the centerline and increase towards the jet edges. Also, transit times of entrained organisms within the jets are short, of the order of seconds, and vary according to where along the trajectory they are entrained and how they wander within the jet.

In the following we take several approaches to this problem. In Sections 6.3 and 6.4 we discuss turbulence characteristics of jets and estimate turbulence length scales for the various brine discharge scenarios. We estimate the total volumes where effects may be expected and express it as a fraction of the total volume of the BMZ. Then we estimate the fraction of the ambient flow that passes over the diffuser that is entrained, and therefore the fraction of larvae entrained. Finally, in Section 6.5, we estimate the total numbers of organisms entrained by the diffuser and the number that may be subject to mortality.

6.2 Plankton Field Data

In order to estimate planktonic levels, seawater samples were taken on May 14, 2016 along the three towed transects shown in Figure 16. The results are summarized by taxonomic group and size ranges in Table 9.

Figure 16. Transect lines for plankton samples 5/14/16.

Table 9. Summary of Plankton Tows Monterey May 14, 2016

Taxonomic Group		Size (mm)	Count (#/m^3)
Copepods	Copepod_unid	0.3 - 5.0	33.73
	Calanoid	1.0 - 5.0	3052.72
	Oithona_sp	0.5 - 2.0	369.85
	Corycaeus_sp	0.3 - 1.5	64.31
	Copepod_nauplii	0.1 - 0.2	77.69
		Copepod total	3598.29
Other	Euphausiid_nauplii	0.35 - 0.5	13.99
	Euphausiid_Calyptopis	0.8 - 2.2	613.94
	Euphausiid_furcilia	1.0 - 5.6	79.68
	Cirripedia_nauplii	0.35 - 0.5	13.83
	Pleurobrachia_sp	2.0 - 10.0	3.93
	Cladocera_podon	0.2 - 3.0	2.83
	Salp	1.0 - 10.0	79.46
	Appendicularia_unid	1.0 - 1.5	58.04
	Oikopleura_unid	1.0 - 1.5	13.83
	Chaetognath_unid	4.0 - 10.0	29.69
	Isopod_unid	0.4 - 1.0	1.97
	Polychaete_unid	0.5 - 5.0	4.71
	Polychaete_trochophore	0.2 - 0.8	2.67
	Decapod_zoea	2.0 - 5.0	4.40
	Gastropod_larvae	0.8 - 3.0	3.30
	Bivalve_veliger	0.75 - 1.0	4.08
	Siphonophore	1.0 - 5.0	7.07
	Hydromedusa	0.5 - 10	1.41
		Other total	938.82
		Overall total	4537.11

6.3 Jet Turbulence and Entrainment

The turbulence generated by the diffuser is discussed below, in particular the spatial variations of turbulence intensity and length scales (eddy sizes) of the turbulence. The diffuser discharges are initially horizontal and have relatively flat trajectories (Figures 8, 9, and 11) so it reasonable to analyze them as pure jets (i.e. flows driven by momentum only).

The properties of jets are well known, and summarized for example in Fischer et al. (1979). An LIF image of a jet and a depiction of its main features are shown in Figure 17. Closer to the nozzle the jet is more fine-grained but the turbulent scales increase along its trajectory. External flow is entrained into the jet (and dilutes it) and the jet width increases linearly with distance from the nozzle.

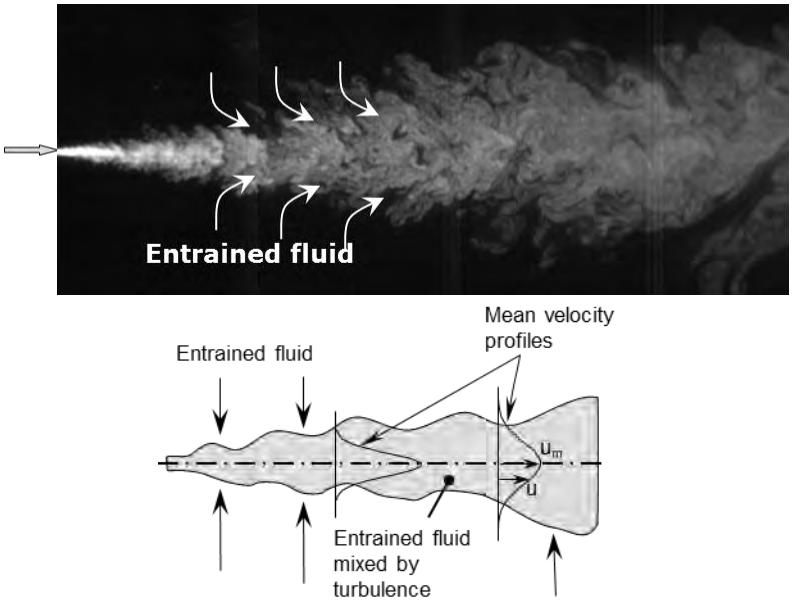

Figure 17. LIF image and main properties of a jet

Beyond the zone of flow establishment, which is about 6*d* long, the centerline velocity u_m decreases rapidly with distance *x* according to:

$$u_m = 6.2u\frac{d}{x} \tag{4}$$

where *u* is the jet velocity and *d* the diameter. The half-width of the jet *w*, defined as two standard deviations of a Gaussian velocity distribution, increases linearly with distance according to:

$$w = 0.15x \tag{5}$$

Combining Eqs. 4 and 5, we see that the average mean shear in the jet $d\bar{u}/dr$ where $\bar{u}$ is the local velocity and *r* the radial distance is:

$$\frac{d\bar{u}}{dr} \approx \frac{u_m}{w} \approx 41\frac{ud}{x^2} \tag{6}$$

So it decreases even more rapidly than velocity with distance from the nozzle. Note that the mean shear on the jet centerline is zero.

The turbulence properties in the jet can be estimated from the experimental data of Webster et al. (2001). They show that the relative turbulence intensity on the centerline, $\tilde{u}/u_m \approx 0.3$ where $\tilde{u}$ is the rms value of the turbulent velocity fluctuations. The intensity decreases with radial distance to zero at the edge of the jet, defined approximately by Eq. 5.

The size of the small-scale (Kolmogorov) eddies η can be estimated from:

$$\eta \sim \left(\frac{\nu^3}{\varepsilon} \right)^{1/4} \tag{7}$$

where ν is the kinematic viscosity of seawater and ε the energy dissipation rate, that can be approximated as:

$$\varepsilon \sim \frac{\tilde{u}^3}{l_L} \tag{8}$$

where l_L is a measure of the largest (energy containing) eddies in the jet. According to Wygnanski and Fiedler (1969) these length scales also increase linearly with distance from the nozzle and vary radially across the jet. On the centerline, $l_L \sim 0.016x$, i.e. about 1/12 of the jet width.

Finally, combining the above equations we find:

$$\frac{\eta_c}{x} = 0.24\,\mathrm{Re}^{-3/4} \tag{9}$$

where $\mathrm{Re} = ud/\nu$ is the jet Reynolds number and η_c the size of the Kolmogorov eddies on the jet centerline. The Kolmogorov scale therefore increases linearly along the jet trajectory.

The radial variation of turbulence intensity and turbulent length scales across the jet is now considered. Near the jet edge, $l_L \sim 0.03x$ according to Wygnanski and Fiedler, i.e. about 1/25 of the jet width, and the turbulence intensity is about $\tilde{u}/u_m \approx 0.04$ according to Webster et al. (2001). Combining Eqs. 7 and 8 we can estimate the ratio of the Kolmogorov scale on the centerline to that at the jet edge as:

$$\frac{\eta_c}{\eta_e} = \left\{ \frac{\left(\ell_c/\ell_e\right)}{\left(\tilde{u}_c/\tilde{u}_e\right)^3} \right\}^{1/4} \approx 0.2 \tag{10}$$

where the subscripts *c* and *e* refer to the jet centerline and edge, respectively. Eq. 10 indicates that the Kolmogorov scales at the jet edge are about five times larger than on the centerline.

Travel times of entrained larvae along the jet trajectory will vary, depending on where along the trajectory they enter the jet and whether they mainly travel on the centerline, on the edge, or in between. On the centerline, the velocity decreases according to Eq. 4 so the travel time along the trajectory to the impact point is given approximately by:

$$t = \int_0^L \frac{dx}{u_m} = \int_0^L \frac{x}{6.2ud} dx = \frac{L^2}{12.4ud} \tag{11}$$

where *L* is the length of the trajectory from the nozzle to the seabed impact point.

As previously discussed, the jet properties were predicted by UM3 (Table 7). In addition, the diameters of the jets at impact d_j were obtained and the volumes of the 129 jets computed, assuming them to be conical up to impact:

$$V_j = 129 \times \frac{d_j^2 L}{12} \tag{12}$$

This volume was computed as a fraction of the water volume in the BMZ, V_{BMZ}, computed from:

$$V_{BMZ} = L \times w_{BMZ} \times H + \pi \left(\frac{w_{BMZ}^2}{4} \right) \times H = 10^8 \ \text{ft}^3 \tag{13}$$

where L = 1024 ft is the diffuser length, w_{BMZ} = 656 ft (200 m) is the width of the brine mixing zone, and H = 104 ft is the average water depth at the diffuser.

In desalination projects, the word entrainment arises in two contexts. It refers to flow drawn into intakes, and, in the jets and plumes that arise in brine diffusers, it refers to the flow induced by velocity shear at the edge of the jet (see Figure 17). This flow, commonly referred to as entrained flow, mixes with and dilutes the effluent stream. Below we consider the magnitude and spatial variation of the entrained velocity and the magnitude of the entrained flow expected to be subjected to significant shear and turbulence effects.

The velocity at which flow is entrained into the jet is directly proportional to the local centerline velocity and is given by:

$$u_o = \alpha u_m \tag{14}$$

where u_o is the entrainment velocity at a radial distance $r = b_w$ from the jet centerline and b_w is defined from the usually assumed radial velocity variation:

$$\frac{u_r}{u_m} = \exp\left\{ -\frac{r^2}{b_w^2} \right\} \tag{15}$$

where u_r is the entrainment velocity at radial distance r. The length scale b_w grows linearly with x according to (Fischer et al. 1979):

$$b_w = 0.107 x \tag{16}$$

The variation of the entrained velocity u_e with radial distance r beyond the edge of the jet can be determined by continuity:

$$u_o 2\pi b_w = u_e 2\pi r$$

or

$$u_e = u_o \frac{b_w}{r} \tag{17}$$

i.e. the entrained velocity decreases rapidly with distance from the jets in inverse proportion to the distance *r*.

Combining Eqs. 4, 13, 15, and 16, we find:

$$u_e = 6.2 \times 0.107 \alpha \frac{ud}{r}$$

Assuming α = 0.0535 (Fischer et al., 1979), this becomes:

$$u_e = 0.035 \frac{ud}{r} \tag{18}$$

In other words, the entrainment velocity is constant with *x*, the distance along the jet, but decreases rapidly away from the jet in the radial direction. The entrainment velocity at any location depends only on the source momentum flux of the jet, which is proportional to *ud*.

Now we apply this result to case P2. From Table 7, *u* = 8.9 ft/s, and *d* = 1.87 in, yielding:

$$u_e = \frac{0.049}{r} \quad \text{ft/s} \tag{19}$$

So, at a distance of 3 ft from the jet centerline, the velocity has fallen to about 0.02 ft/s (0.5 cm/s), already much smaller than typical oceanic velocities.

The total volume entrained into the jets is directly related to dilution. It is given by (Fischer et al. 1979):

$$Q_E = Q \times S_a \tag{20}$$

where *Q* is the source discharge rate and S_a the average dilution. The average dilution $S_a = 1.4 S_m$ where S_m is the minimum centerline dilution. So a centerline dilution of 16:1 requires entraining about 22 times the source flow rate.

The total flux of water passing over the diffuser and BMZ can be estimated from:

$$Q_{BMZ} = \bar{U} \times \left(L + 2 w_{BMZ} \right) \times H \tag{21}$$

where $\bar{U}$ is the mean oceanic drift speed. The ADCP measurements of Tenera (2014) at a depth of 30 m near the mouth of the Monterey Canyon imply a mean drift speed of about 5 cm/s.

6.4 Results and Discussion

The main flow properties for the various dense discharge scenarios of Tables 6 and 7 were computed according to Eqs. 9 through 21. The results are summarized in Table 10 where the kinematic viscosity ν was assumed to be 1.2×10^{-5} ft^2/s and the mean oceanic drift speed $\bar{U} = 5$ cm/s. In addition, estimates of scales, dilution

and entrainment for the baseline domestic wastewater discharge (Case P1, 19.78 mgd) are also shown.

For case P2 (pure brine), the Kolmogorov scale on the centerline ranges from about 0.012 mm near the nozzle to 0.14 mm at the impact point. At the jet edge it therefore ranges from about 0.06 mm near the nozzle to about 0.7 mm. The mean shear rates range from about 57 sec^{-1} near the nozzle to 0.4 sec^{-1} at the impact point.

The maximum centerline travel time is about 8 seconds. The mean velocity profiles of Webster et al. (2001) show that the jet velocity is greater than about 20% of the maximum over about 80% of the jet width. Therefore, closer to the jet edges, travel times will be around 40 seconds. Organisms entrained and traveling near the jet edges will undergo lower intensities (larger eddies) but for longer times.

Clearly, the Kolmogorov scales in the jet will be smaller to or comparable than the smallest organisms of interest (Table 9). They range from 0.012 to 2.5 mm. These are mostly somewhat smaller than the Kolmogorov scale due to natural turbulence in the ocean which in Monterey is about 1 mm (Walter et al. 2014). Therefore, the Kolmogorov scale of the natural turbulence is also comparable to larvae size and may cause natural mortality. The incremental mortality due to the jets are estimated below.

In turbulence, there is a continuous spectrum of eddy sizes and turbulent kinetic energy from the smallest (Kolmogorov) to the largest (energy-containing) eddies. For case P2, they range from about 0.01 mm to 0.24 m, so there will be some eddies of size comparable to the organism sizes that may affect them. It should be noted, however, that the strain rates (and shear stresses) are maximum at the Kolmogorov scale and decrease as the eddy size increases.

The volume of water in the jets where turbulent intensities are greater than background is almost infinitesimally small compared to the volume of the BMZ. It ranges from 0.006% for case P2 to 0.4% for case V9.

For the brine discharges, only a small fraction of the water passing over the diffuser is entrained. It ranges from 1.7% for case P2 to 6.4% for case V9. This estimate depends on the assumed value of the oceanic drift speed, conservatively assumed to be 5 cm/s. For higher speeds it would be less.

The area of high shear impacted by the diffusers is relatively small and transit times through this region relatively short. Thus, it seems reasonable to expect that, while the larvae that experience the highest shear may experience lethal damage, the overall increase in mortality integrated over the larger area will be low.

The volumes entrained into the brine discharges are much less than into the baseline (P1) case. This is mainly because the dilutions for the baseline case is much higher. For the brine discharges the entrainment rates range from 7 to 22% of those for the baseline case. Therefore, organism mortality for the brine discharges would also be expected to be about 7 to 22% of the baseline case.

Table 10. Summary of Turbulence and Entrainment Calculations

Case No.	Effluent		Port conditions			UM3 predictions					Travel time center-line	Total volume as % of BMZ	Kolmogorov scales		Entrained flows	
	Flow	Density	Velocity	Diam.	Reynolds number ($x10^{-5}$)	Dilution	Impact distance	Diam-eter	Traj-ectory	Volume			At 1 ft	At impact	Volume	As % of BMZ flux
	(mgd)	(kg/m^3)	(ft/s)	(in)			(ft)	(in)	(ft)	(ft^3)	(sec)		(mm)	(mm)	(mgd)	
P1	19.78	998.8	10.0	1.96	1.36	191	-	-	-	-	-	-	0.01	-	5290	28.5
P2	13.98	1045.2	8.9	1.87	1.16	16.3	10.3	49	12.0	52.4	8.4	0.0064	0.012	0.140	319	1.7
P3	14.98	1041.2	8.9	1.86	1.14	16.9	10.7	51	12.5	59.1	9.1	0.0073	0.012	0.146	354	1.9
P4	15.98	1038.5	9.2	1.89	1.21	17.8	11.8	56	13.6	78.3	10.2	0.0096	0.011	0.153	398	2.1
P5	22.98	1026.4	11.2	2.07	1.62	35.3	29.0	140	31.9	1137.0	42.3	0.1397	0.009	0.290	1136	6.1
P6	33.76	1017.6	14.8	2.28	2.35	-	-									
V1	8.99	1045.2	7.4	1.67	0.86	16.3	8.7	41	10.4	31.7	8.5	0.0039	0.015	0.152	205	1.1
V2	9.99	1040.5	7.7	1.70	0.91	17.4	9.8	46	11.5	43.6	9.9	0.0054	0.014	0.161	243	1.3
V3	10.99	1036.6	7.6	1.71	0.91	18.5	10.9	50	12.7	58.4	11.9	0.0072	0.014	0.177	285	1.5
V4	14.79	1026.4	9.0	1.88	1.18	32.5	24.0	116	26.5	644.3	40.2	0.0792	0.012	0.305	673	3.6
V5	28.77	1012.7	13.5	2.21	2.07	-	-									
V6	9.93	1041.1	7.7	1.70	0.91	17.2	9.7	46	11.4	44.0	9.7	0.0054	0.014	0.160	239	1.3
V7	10.93	1036.5	7.9	1.74	0.95	18.2	10.9	52	12.7	61.7	11.3	0.0076	0.014	0.171	278	1.5
V8	12.93	1030.6	8.4	1.80	1.05	22.1	14.7	70	16.6	147.1	17.7	0.0181	0.013	0.208	400	2.2
V9	15.23	1026.1	9.0	1.88	1.17	55.4	42.1	204	46.1	3473.9	121.5	0.4268	0.012	0.531	1181	6.4
V10	25.85	1014.7	12.6	2.16		-	-									

6.5 Plankton Entrainment and Mortality

Estimated rates of organism entrainment into the jets were computed as a product of the entrained volumes from Table 10 and organism concentrations in in Table 9. The results are shown in Table 11, sorted by organism size from smallest to largest. Although the absolute numbers of entrained organisms are high, they represent only a small fraction of those passing over the diffuser, which is similar to the fraction of water entrained: about 2 to 6% according to Table 10.

Because the natural Kolmogorov scale near the diffuser is about 1 mm, it is argued that incremental mortality due to the jets will only occur for regions where the Kolmogorov scale is shorter than this and by organisms smaller than 1 mm. We assume no incremental mortality for organisms larger than 1 mm. Organisms smaller than 1 mm comprise only 27% of the total, and the fraction of them that actually die is uncertain. According to the literature it could be anywhere from zero to about 50%; we assume the conservative upper limit of 50%. The results are summarized in Table 11.

We emphasize that 50% is most probably a very conservative upper limit to the fractional mortality. As discussed, organisms in a jet are subject to its turbulence for only brief periods of seconds and the turbulence intensity decreases rapidly as they travel through the jet.

It is useful to combine these estimates to obtain an upper bound for the fraction of entrained organisms passing over the diffuser that may be subject to mortality. For case P2, we have, from Tables 10 and 11.

$$\begin{pmatrix}\text{Fraction of}\\ \text{BMZ flux}\\ \text{entrained}\end{pmatrix}\times\begin{pmatrix}\text{Fraction of}\\ \text{organisms}\\ <1\text{ mm}\end{pmatrix}\times\begin{pmatrix}\text{Fraction}\\ \text{mortality}\end{pmatrix}=0.017\times0.266\times0.50=0.0023=0.23\%$$

Note that similar calculations are made for intakes. For example, Tenera (2014) estimated larvae entrainment into a proposed intake near the head of the Monterey Canyon. Because intakes are essentially point sinks, the concept of water flux passing over them is meaningless so the methods used here do not apply. They use the ETM (Empirical Transport Model) approach whereby the proportional mortality of larvae in the source water population is estimated. They estimate the highest estimated proportional mortality to be of order 0.1% for a 63 mgd intake. For the diffuser, the volumes entrained for dilution are about 5 to 20 times this amount so if the same approach were used here approximately 0.5 to 2.0% of the source flow would be subject to mortality, similar to that estimated in Table 10. The difference of course is that 100% mortality of entrained organisms is assumed for intakes whereas a much smaller fraction, if any, larvae die in passing through the jets.

Table 11. Estimates of entrainment and mortality. Organisms sorted by size, small to large. Case P2

Taxonomic Group		Size (mm)	Count (#/m^3)	% of total	Cumulative %	Entrainment (#/day)	Incremental mortality (#/day)
Copepods	Copepod_nauplii	0.1 - 0.2	77.69	1.71	1.71	114,680,910	57,340,455
Other	Cladocera_podon	0.2 - 3.0	2.83	0.06	1.77	4,172,099	2,086,050
Other	Polychaete_trochophore	0.2 - 0.8	2.67	0.06	1.83	3,940,942	1,970,471
Copepods	Copepod_unid	0.3 - 5.0	33.73	0.74	2.58	49,790,726	24,895,363
Copepods	Corycaeus_sp	0.3 - 1.5	64.31	1.42	3.99	94,933,608	47,466,804
Other	Euphausiid_nauplii	0.35 - 0.5	13.99	0.31	4.30	20,649,175	10,324,588
Other	Cirripedia_nauplii	0.35 - 0.5	13.83	0.30	4.61	20,409,510	10,204,755
Other	Isopod_unid	0.4 - 1.0	1.97	0.04	4.65	2,902,172	1,451,086
Copepods	Oithona_sp	0.5 - 2.0	369.85	8.15	12.80	545,978,077	272,989,039
Other	Polychaete_unid	0.5 - 5.0	4.71	0.10	12.91	6,953,004	3,476,502
Other	Hydromedusa	0.5 - 10	1.41	0.03	12.94	2,086,050	1,043,025
Other	Bivalve_veliger	0.75 - 1.0	4.08	0.09	13.03	6,026,992	3,013,496
Other	Euphausiid_Calyptopis	0.8 - 2.2	613.94	13.53	26.56	906,316,100	453,158,050
Other	Gastropod_larvae	0.8 - 3.0	3.30	0.07	26.63	4,868,389	2,434,194
Copepods	Calanoid	1.0 - 5.0	3052.72	67.28	93.91	4,506,487,870	0
Other	Euphausiid_furcilia	1.0 - 5.6	79.68	1.76	95.67	117,622,706	0
Other	Salp	1.0 - 10	79.46	1.75	97.42	117,305,750	0
Other	Appendicularia_unid	1.0 - 1.5	58.04	1.28	98.70	85,679,028	0
Other	Oikopleura_unid	1.0 - 1.5	13.83	0.30	99.01	20,418,019	0
Other	Siphonophore	1.0 - 5.0	7.07	0.16	99.16	10,430,248	0
Other	Pleurobrachia_sp	2.0 - 10	3.93	0.09	99.25	5,804,344	0
Other	Decapod_zoea	2.0 - 5.0	4.40	0.10	99.35	6,492,125	0
Other	Chaetognath_unid	4.0 - 10	29.69	0.65	100.00	43,832,517	0
		Totals	4537.11			6,697,780,360	891,853,877

7. DILUTION MITIGATION

7.1 Introduction

This section explores methods to increase dilution for dense discharges (brine, and brine comingled with secondary and GWR effluents). In particular, it has been suggested that some combinations of effluents may not achieve sufficient dilution to meet the water quality requirements of the Ocean Plan. Particularly troublesome may be ammonia levels when low to moderate volumes of secondary effluent are added to brine. Trussell (2016) identifies some cases, reproduced in Table 12, where the dilutions predicted from Tables 7 and 8 are insufficient to achieve the target goals of 80% of the compliance limit. Note that the dilution D_m used in Table 9 is $D_m = S_m - 1$ where S_m is the dilution in Tables 7 and 8 to agree with the definition of dilution used in the Ocean Plan. It can be seen that cases V6, V7, and V8 may not achieve sufficient dilution.

Table 12. Minimum Dms required for Variant Project with GWR concentrate flow (Trussell, 2016)

Case No.	Minimum required Dm for compliance				Modeled Dm		
	WW flow (mgd)	50% of Dm required	80% of Dm required	100% of Dm required	Cederwall	UM3	NRFIELD
V6	0.0	69	37	30	15.6	16.2	-
V7	1.0	65	41	32	16.4	17.2	-
V8	3.0	73	46	37	21.6	22.2	-
V9	5.3	80	50	40	76.6	55.0	-
V10	15.9	96	60	48	-	194	220

Several possible mitigation strategies have been suggested to increase dilution:

1. Augment the discharges by adding treated RO water to the brine from the GWR or desalination facility. This would increase the jet velocities and decrease the density difference between the effluent and receiving water, both of which will increase dilution.
2. Increase the flow per port by either temporarily storing on site in a storage basin and pumping briefly at higher flow rates, or by closing off some ports. Both would increase the jet velocity and increase dilution.
3. Discharge through upwardly inclined nozzles either by retrofitting the existing horizontal nozzles or by constructing a new dedicated brine diffuser.

These options are analyzed in this section, focusing on cases V6, V7, and V8. In addition, the effect of retrofitting upward nozzles on the MRWPCA diffuser on

the dilution of positively buoyant discharges is discussed along with some engineering issues.

7.2 Flow Augmentation

In this scenario, flows with densities close to freshwater are added to the brine and secondary effluent mixtures to increase jet velocity and decrease the density difference between the combined effluent and the receiving water.

The following procedure was followed to analyze this scenario. A quantity of water was added to the base flow and the new flow rate and effluent density were computed. The internal hydraulics program was then run and the variations in effective port diameter and flow per port along the diffuser were obtained. The calculations account for the variation of port opening with flow as explained in Appendix A. Dilution calculations were then performed for the ports with highest and lowest flows and the lowest value of dilution chosen. The dilution calculations were performed using the Cederwall equation (Eq. 3), and UM3 was also run for some cases to determine jet trajectories.

The results are plotted as functions of flow added in Figure 18 and are summarized in Table 13. The effect of added flow on the jet trajectories predicted by UM3 is shown in Figure 19 for two typical cases: V6.10 and V6.14.

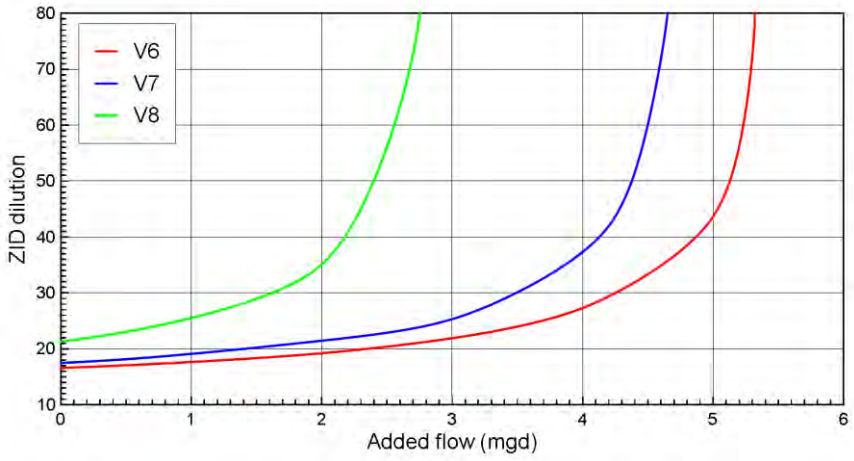

Figure 18. Effect on dilution of added freshwater flows to cases V6, V7, and V8.

Table 13. Effect of added flow on dilution for selected scenarios

Case No.	Background density	Makeup Flow	Combined flow		Port conditions							Dilution by Cederwall formula
			Flow	Density	Flow		Diam.	Height	Velocity	Froude no.	y/dF	
	(kg/m^3)	(mgd)	(mgd)	(kg/m^3)	(gpm)	(cfs)	(in)	(ft)	(ft/s)			
V6.10	1025.8	0.0	9.9	1041.1	54.3	0.121	1.70	4.0	7.7	29.5	0.96	16.6
V6.11	1025.8	0.5	10.4	1039.0	56.3	0.126	1.72	4.0	7.8	32.0	0.87	17.0
V6.12	1025.8	1.0	10.9	1037.2	58.8	0.131	1.74	4.0	7.9	34.9	0.79	17.6
V6.13	1025.8	2.0	11.9	1033.9	58.6	0.131	1.74	4.0	7.9	41.3	0.67	19.2
V6.14	1025.8	3.0	12.9	1031.1	63.9	0.142	1.78	4.0	8.2	52.6	0.51	21.9
V6.15	1025.8	4.0	13.9	1028.7	72.4	0.161	1.84	4.0	8.7	74.3	0.35	27.3
V6.16	1025.8	5.0	14.9	1026.7	76.3	0.170	1.87	4.0	8.9	136.2	0.19	43.7
V6.17	1025.8	5.3	15.2	1026.1	77.8	0.173	1.88	4.0	9.0	243.6	0.10	72.6
V7.10	1024.8	0.0	10.9	1036.5	58.3	0.130	1.74	4.0	7.9	34.2	0.81	17.4
V7.11	1024.8	0.5	11.4	1034.8	57.2	0.128	1.73	4.0	7.8	36.7	0.76	18.1
V7.12	1024.8	1.0	11.9	1033.2	60.2	0.134	1.75	4.0	8.0	41.0	0.67	19.1
V7.13	1024.8	2.0	12.9	1030.5	66.5	0.148	1.80	4.0	8.4	51.2	0.52	21.4
V7.14	1024.8	3.0	13.9	1028.2	67.3	0.150	1.81	4.0	8.4	66.3	0.40	25.3
V7.15	1024.8	4.2	15.1	1025.8	77.3	0.172	1.87	4.0	9.0	129.8	0.20	42.0
V7.16	1024.8	4.6	15.5	1025.1	78.8	0.176	1.88	4.0	9.1	241.4	0.11	72.0
V7.17	1024.8	4.75	15.7	1024.8	78.8	0.176	1.88	4.0	9.1	1283.9	0.02	353.5
V8.10	1024.8	0.0	12.9	1030.6	66.5	0.148	1.80	4.0	8.4	50.6	0.53	21.3
V8.11	1024.8	0.5	13.4	1029.4	69.3	0.155	1.82	4.0	8.6	57.8	0.46	23.0
V8.12	1024.8	1.0	13.9	1028.3	72.6	0.162	1.84	4.0	8.8	67.5	0.39	25.5
V8.13	1024.8	2.0	14.9	1026.3	76.3	0.170	1.87	4.0	8.9	104.1	0.25	35.1
V8.14	1024.8	2.5	15.4	1025.3	78.3	0.175	1.88	4.0	9.1	182.6	0.14	56.1
V8.15	1024.8	2.8	15.7	1024.8	78.3	0.175	1.88	4.0	9.1	1291.0	0.02	355.4

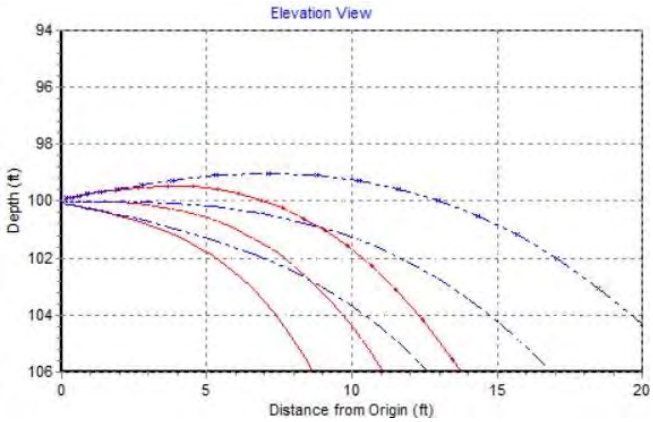

Figure 19. Jet trajectories predicted by UM3 for flow cases V6.10 (red) and V6.14 (blue).

The higher jet velocity and smaller density differences leads to a flatter and longer trajectory and therefore higher dilution. Of these, the main effect is due to the decreased density difference because the ports open as the flow increases, offsetting the increased jet velocity that would occur for a fixed office.

For low added volumes the effect on dilution is small. As the flow increases to where the density of the combined effluent approaches that of the background, i.e. the flow becomes neutrally buoyant, the dilution increases exponentially. It becomes theoretically infinite as for this case the jet trajectory is then horizontal and the jet centerline does not impact the seabed. For the three cases considered, the additional volumes required to satisfy the dilution requirements of Table 12 and the volumes for neutral buoyancy are summarized in Table 14.

Table 14. Effect of added freshwater volumes

Case No.	Base flow	For 80% compliance		Additional flow for neutral buoyancy
		Dilution needed	Additional flow	
	(mgd)		(mgd)	(mgd)
V6	9.9	38	4.8	5.5
V7	10.9	42	4.2	4.8
V8	12.9	47	2.3	2.8

Note that the actual volumes required to achieve the water quality requirements would be slightly less than those given in Table 14 due to "in-pipe" dilution by the added flow that will reduce the source concentrations.

7.3 Varied Port Flow

This mitigation technique varies the flow per port. This can be accomplished either by holding the effluent temporarily in a storage basin and then pumping intermittently at higher flow rates or by closing some of the open ports or opening some of the closed ports. More port flow increases the jet exit velocity which increases entrainment and increases the jet trajectory length thereby increasing dilution. Because these strategies are essentially identical in terms of their effect on dilution, only the former case is analyzed here. The results can also be used to estimate the effects of opening or closing ports. There are presently 129 open ports and 42 closed ports. So opening all ports would result in a reduction in the flow per port by 25%. This case is included below.

The procedure is similar to that of the previous section. A pumping rate was assumed and the internal hydraulics program was run. The highest and lowest port flows and their diameters were obtained and dilution calculations run for both. The lowest was chosen. For each pumping rate, the composition of the effluent, i.e. its density, was assumed constant and equal to that of the base cases.

The resulting dilutions are plotted as a function of pumping rate in Figure 20 and summarized in Table 15. The effect of increased flow on jet trajectory predicted by UM3 is shown for two typical cases in Figure 21.

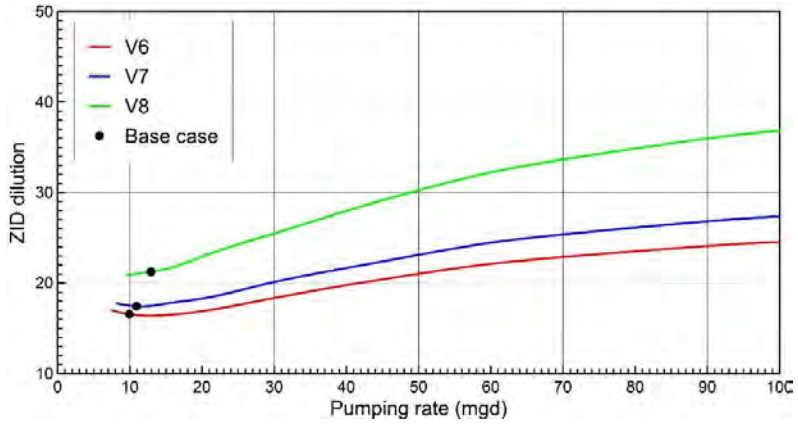

Figure 20. Effect of pumping rate on dilution for flow cases V6, V7, and V8.

The increased jet velocity leads to a longer and flatter trajectory leading to increased dilution at the impact point. However, as the flow increases, the port opening also increases, offsetting the increased jet velocity.

The dilution increases quite slowly in response to increased flow rate and the required dilutions cannot be achieved for flows below about 100 mgd, where the head required would exceed 50 ft. Note that the effect on dilution of closing ports is the same and can be readily estimated. For example, a doubling of the pumping rate is equivalent to closing half the ports.

Table 15. Effect of added flow on dilution for selected scenarios

Case No.	Background density	Effluent		Port conditions							Dilution by Cederwall formula
		Flow	Density	Flow		Diam.	Height	Velocity	Froude no.	y/dF	
	(kg/m^3)	(mgd)	(kg/m^3)	(gpm)	(cfs)	(in)	(ft)	(ft/s)			
V6.20	1025.8	9.9	1041.1	54.3	0.121	1.70	4.0	7.7	29.5	0.96	16.6
V6.21	1025.8	12.0	1041.1	64.8	0.145	1.79	4.0	8.3	30.9	0.87	16.4
V6.22	1025.8	15.0	1041.1	75.1	0.167	1.86	4.0	8.9	32.6	0.79	16.5
V6.23	1025.8	20.0	1041.1	103.3	0.230	2.01	4.0	10.5	36.9	0.65	16.9
V6.24	1025.8	30.0	1041.1	160.5	0.358	2.21	4.0	13.4	45.2	0.48	18.3
V6.25	1025.8	40.0	1041.1	207.8	0.463	2.32	4.0	15.8	51.8	0.40	19.8
V6.26	1025.8	60.0	1041.1	308.3	0.688	2.52	4.0	19.8	62.5	0.30	22.1
V6.27	1025.8	100.0	1041.1	505.3	1.127	2.87	4.0	25.1	74.1	0.23	24.5
V7.20	1024.8	10.9	1036.5	58.3	0.130	1.74	4.0	7.9	34.2	0.81	17.4
V7.21	1024.8	12.0	1036.5	59.4	0.132	1.75	4.0	7.9	34.3	0.80	17.4
V7.22	1024.8	15.0	1036.5	76.0	0.169	1.86	4.0	9.0	37.7	0.68	17.7
V7.23	1024.8	20.0	1036.5	105.3	0.235	2.02	4.0	10.6	42.5	0.56	18.3
V7.24	1024.8	30.0	1036.5	161.4	0.360	2.21	4.0	13.5	52.0	0.42	20.1
V7.25	1024.8	40.0	1036.5	206.8	0.461	2.32	4.0	15.7	59.1	0.35	21.7
V7.26	1024.8	60.0	1036.5	307.3	0.685	2.52	4.0	19.8	71.4	0.27	24.5
V7.27	1024.8	100.0	1036.5	609.7	1.360	3.08	4.0	26.3	85.7	0.18	27.3
V8.20	1024.8	12.9	1030.6	66.5	0.148	1.80	4.0	8.4	50.6	0.53	21.3
V8.21	1024.8	15.0	1030.6	77.8	0.173	1.88	4.0	9.0	53.1	0.48	21.6
V8.22	1024.8	20.0	1030.6	105.9	0.236	2.02	4.0	10.6	60.4	0.39	22.9
V8.23	1024.8	30.0	1030.6	154.8	0.345	2.19	4.0	13.2	72.1	0.30	25.5
V8.24	1024.8	40.0	1030.6	205.3	0.458	2.32	4.0	15.6	82.8	0.25	28.0
V8.25	1024.8	60.0	1030.6	305.8	0.682	2.52	4.0	19.7	100.3	0.19	32.2
V8.26	1024.8	100.0	1030.6	500.8	1.117	2.86	4.0	25.0	119.7	0.14	36.8

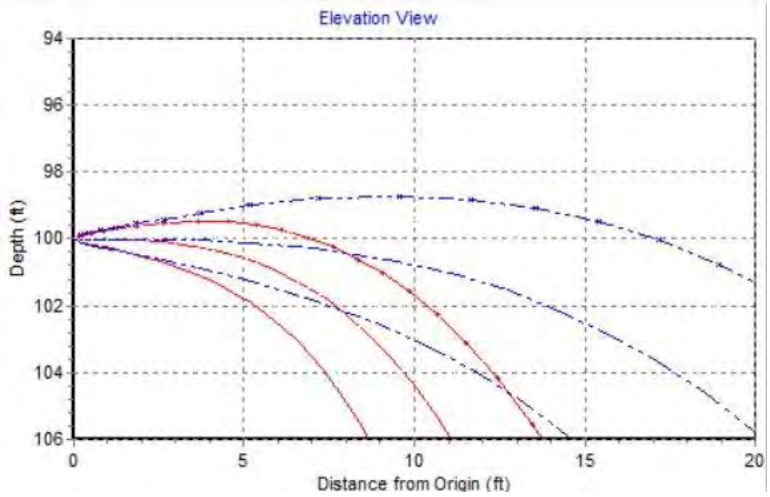

Figure 21. Jet trajectories predicted by UM3 for flow cases V7.10 (red) and V7.14 (blue).

The reason for this seemingly paradoxical result is that the dilution for these cases is primarily a result of jet-induced entrainment. For a pure jet (i.e. a flow with neutral buoyancy) from a fixed orifice the flow, jet velocity, and entrained flow all increase in direct proportion to each other. The dilution at any distance from the nozzle, which is the ratio of the entrained flow to the source flow, therefore remains constant and is dependent only on the nozzle diameter (Fischer et al. 1979). In other words, increasing the flow for a pure jet does not increase dilution at a fixed point.

Dilution at the seabed does increase for the present cases as the flow increases, however, due to the longer jet trajectory before impacting the seabed as shown in Figure 21. The effect is again mitigated, however, by the variable opening of the nozzles: as the flow increases, the increase in jet velocity is much less than for a fixed orifice. Similarly, reducing the flow per port by opening closed ports does not result in a significant change in dilution. A fixed orifice would result in longer trajectories and higher dilutions than found above, but the head required would probably be prohibitive. It is clear that varying the flow per port either by pumping at a higher rate or opening or closing ports is not an effective strategy for increasing dilution.

7.4 Effect of Inclined Nozzles

7.4.1 Introduction

Diffusers for discharging dense effluents normally consists of nozzles that are inclined upwards. The optimum angle to the horizontal is 60° (Roberts and Abessi, 2014) as this maximizes the jet path length and dilution at the impact point. Such jets have been extensively studied and a typical flow image is shown in Figure 22. As shown in the definition diagram, the jet reaches a terminal rise height y_t and

then falls back to the seabed. The impact dilution, S_i, interpreted here as the ZID dilution, is where the jet centerline intersects the seabed.

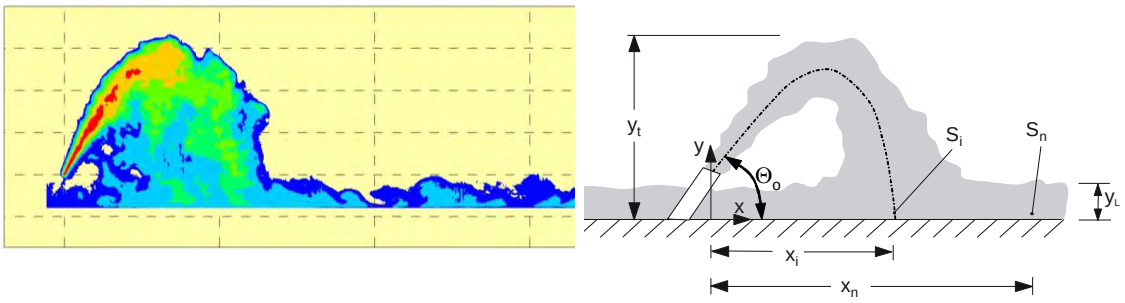

LIF image **Definition diagram**

Figure 22. Laser Induced Fluorescence (LIF) image of a 60° jet and definition diagram.

Inclined jets can be achieved either by retrofitting the existing check valves with upwardly inclined nozzles or by building a dedicated brine outfall and diffuser. The analyses are similar and both are considered below. Also discussed is the effect on dilution of positively buoyant effluents of retrofitting with inclined jets.

7.4.2 Diffuser Retrofit

The nozzle designs with check valves are shown in Figure A-3 in Appendix A. For the present analysis it was assumed that valves with similar hydraulic characteristics (Figure A-2) were installed but inclined upwards at 60°.

The dilution S_i of a single 60° jet and the terminal rise height y_t can be estimated from (Roberts et al. 1997):

$$\frac{S_i}{F_j} = 1.6 \tag{22}$$

and

$$\frac{y_t}{dF_j} = 2.2 \tag{23}$$

where F_j is the jet densimetric Froude number (Eq. 2) and d the effective nozzle diameter. These equations have been widely used for brine diffuser designs.

The dilutions and jet rise heights for all the base cases with dense discharges were computed and the results are summarized in Table 16, which can be compared to Table 7. The hydraulics was assumed to be the same as for the horizontal jets.

It is apparent that the inclined jets increase dilution substantially. Dilution for the base case, P2 pure brine, increases from 16:1 to 46:1. All of the required

dilutions for cases V6, V7, and V8 are also met and exceeded. The rise heights of the jets are all less than 100 ft so the jets will always be submerged.

7.4.3 Dedicated Diffuser

A dedicated diffuser for brine discharges would probably consist of multiple nozzles inclined upwards at 60° to the horizontal. (Not vertical as implied in the settlement agreement as vertical jets result in impaired dilution). The nozzles would be either distributed along the sides of the diffuser or clustered in rosette risers as shown in Figure 23.

Figure 23. A brine diffuser with multiport rosettes.

The analysis for the diffuser would be similar to that for the inclined jets above, but it is noted that the outfall and diffuser could be much shorter than the existing outfall. Assuming that the outfall is only used for brine discharges (with all secondary effluent through the MRWPCA outfall), the peak flow would be about 14 mgd, requiring an outfall diameter of around 24 inches. The outfall need not be as long as the MRWPCA outfall as shoreline impact is not a major concern and deep water is not required for dilution. For example (although further analyses would be needed to optimize the outfall and diffuser lengths and nozzle details), the rise height of the jets for the pure brine case in Table 13 is about 10 ft, so the discharge could be into relatively shallow water. Costs for similar outfalls vary widely, but Roberts et al. (2012) quote a median price range for installed outfalls of 24 inch diameter of about $3,700 per meter with a range from $1,000 to $8,000 per meter.

Table 16. Effect of discharge through 60° nozzles

Case No.	Background conditions		Effluent conditions		Port conditions							Equations 4 and 5 at ZID			
												Dilution	Salinity		Rise height
	Salinity	Density	Salinity	Density	Flow		Diam.	Height	Velocity	Froude no.	y/dF		At impact	Incr-ement	
	(ppt)	(kg/m^3)	(ppt)	(kg/m^3)	(gpm)	(cfs)	(in)	(ft)	(ft/s)				(ppt)	(ppt)	(ft)
P1			0.80	998.8											
P2	33.89	1025.8	58.23	1045.2	76.3	0.170	1.87	4.0	8.9	29.0	0.89	46.3	34.41	0.53	9.9
P3	33.34	1024.8	53.62	1041.2	75.0	0.167	1.86	4.0	8.9	31.4	0.82	50.3	33.75	0.40	10.7
P4	33.34	1024.8	50.32	1038.5	80.8	0.180	1.89	4.0	9.2	35.5	0.72	56.8	33.64	0.30	12.3
P5	33.34	1024.8	35.23	1026.4	117.8	0.263	2.07	4.0	11.2	120.3	0.19	192.5	33.35	0.01	45.7
P6	33.34	1024.8	24.24	1017.6	188.5	0.420	2.28	4.0	14.8	71.5	-	-	-	-	-
V1	33.89	1025.8	58.23	1045.2	50.8	0.113	1.67	4.0	7.4	25.6	1.12	40.9	34.48	0.59	7.8
V2	33.89	1025.8	52.48	1040.5	54.3	0.121	1.70	4.0	7.7	30.1	0.94	48.1	34.27	0.39	9.4
V3	33.89	1025.8	47.78	1036.6	54.6	0.122	1.71	4.0	7.6	34.7	0.81	55.6	34.14	0.25	10.9
V4	33.34	1024.8	35.20	1026.4	77.9	0.174	1.88	4.0	9.0	102.0	0.25	163.1	33.35	0.01	35.1
V5	33.89	1025.8	18.75	1012.7	160.8	0.359	2.21	4.0	13.5	48.9	-	-	-	-	-
V6	33.89	1025.8	53.27	1041.1	54.3	0.121	1.70	4.0	7.7	29.5	0.96	47.2	34.30	0.41	9.2
V7	33.34	1024.8	47.78	1036.5	58.3	0.130	1.74	4.0	7.9	34.2	0.81	54.7	33.61	0.26	10.9
V8	33.34	1024.8	40.52	1030.6	66.5	0.148	1.80	4.0	8.4	50.6	0.53	80.9	33.43	0.09	16.7
V9	33.89	1025.8	35.01	1026.1	77.8	0.173	1.88	4.0	9.0	260.5	0.10	416.7	33.89	0.00	89.8
V10	33.34	1024.8	20.67	1014.7	143.3	0.320	2.16	4.0	12.6	52.6	-	-	-	-	-

7.4.4 Effect of Inclined Nozzles on Buoyant Flows

Diffusers for positively buoyant discharges usually have horizontal nozzles (as in the MRWPCA diffuser) as this maximizes jet trajectory and dilution and helps promote submergence. Inclining the nozzles upwards may reduce dilution somewhat. In order to investigate this effect, dilutions for the buoyant discharge scenarios (P1, P6, V5, and V10) of Table 8 were recomputed but with 60° inclined nozzles. The same hydraulic conditions were assumed. Dilution simulations were done with the model UM3 only as NRFIELD assumes horizontal nozzles. The results are summarized in Table 17.

Table 17. Summary of UM3 Dilution Simulations for Buoyant Effluent Scenarios with Horizontal and 60° Nozzles

Case No.	Flow rate (mgd)	Effluent density (kg/m^3)	Port diam. (in)	Ocean condition	Horizontal		60°	
					Average dilution	Rise height (center-line) (ft)	Average dilution	Rise height (center line) (ft)
P1	19.78	998.8	2.00	Upwelling	191	58	184	62
P1	19.78	998.8	2.00	Davidson	327	100 (surface)	310	100 (surface)
P1	19.78	998.8	2.00	Oceanic	240	82	247	91
P6	33.76	1017.6	2.25	Davidson	154	86	142	93
V5	28.77	1012.7	2.18	Upwelling	122	47	111	53
V10	25.85	1014.7	2.13	Davidson	195	100 (surface)	185	100 (surface)

For buoyant discharges of essentially freshwater into fairly deep water the dilution is primarily effected by the buoyancy flux, so the source momentum flux, and therefore the nozzle orientation, is relatively unimportant. This effect is shown in the trajectories predicted by UM3 for case P1 in Figure 24. The trajectory lengths are similar with a slightly higher rise for the inclined jets. The results show small reductions in dilution of about 5% for this case as the trajectory reduction is offset by the increased plume rise height. For case P1 with the Oceanic density profile, the results actually imply a slight increase in dilution with the inclined nozzles due to the increased rise height. For cases P6, V5, and V10 (buoyant discharges with the density difference reduced due to blending with brine), the momentum flux is slightly more important, but even here the dilution reduction is less than 10%

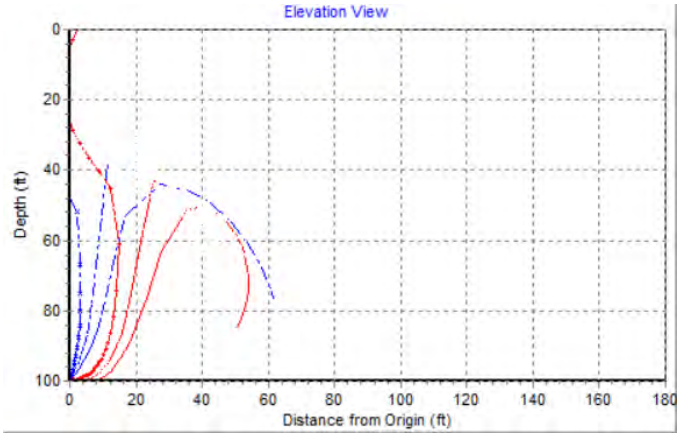

Figure 24. UM3 predicted trajectories for horizontal (red) and 60° inclined (blue) nozzles for case P1 with upwelling density profile.

REFERENCES

Abessi, O., and Roberts, P. J. W. (2014). "Multiport Diffusers for Dense Discharges." J. Hydraul. Eng., http://dx.doi.org/10.1061/(ASCE)HY.1943-7900.0000882, 140(8).

AMS (2016). "Water Column Profiles Assessment at Marina for Monterey Peninsula Water Supply Project Proposed by Cal-Am." Applied Marine Sciences, Technical Memorandum, January 18, 2016.

Cederwall, K. (1968). "Hydraulics of Marine Wastewater Disposal." Report No. 42, Chalmers Institute of Technology, Goteberg, Sweden.

Ding, C. A., Carlson, L., Ellis, C., and Mohseni, O. (2005). "Pressure Loss Coefficients of 6, 8 and 10-inch Steel Pipe Fittings." Project Report 461, St. Anthony Falls Laboratory, University of Minnesota, February 2005.

Fischer, H. B., List, E. J., Koh, R. C. Y., Imberger, J., and Brooks, N. H. (1979). Mixing in Inland and Coastal Waters, Academic Press, New York.

Flow Science (2008) "MRWPCA brine discharge diffuser analysis." FSI 08414, Flow Science, Pasadena California, May 12, 2008.

Flow Science (2014) "MRWPCA brine discharge diffuser analysis - Additional scenarios." FSI 134032, Flow Science, Pasadena California, August 25, 2014.

Frick, W. E., Roberts, P. J. W., Davis, L. R., Keyes, J., Baumgartner, D. J., and George, K. P. (2003). "Dilution Models for Effluent Discharges, 4th Edition (Visual Plumes)." U.S. Environmental Protection Agency, Environmental Research Division, NERL, Standards and Applied Science Division, Office of Science and Technology,

Frick, W. E. (2004). "Visual Plumes mixing zone modeling software." Environmental Modelling & Software, 19, 645-654.

Frick, W. E., and Roberts, P. J. W. (2016). "Visual Plumes 2016: An Updated Public-Domain Plume Model Suite " Proc., International Symposium on Outfall Systems, ISOS2016, IWA. 10 - 13 May 2016.

Isaacson, M. S., Koh, R. C. Y., and Brooks, N. H. (1983). "Plume Dilution for Diffusers with Multiple Risers." J. Hydraul. Eng., 109(2), 199-220.

Kikkert, G. A., Davidson, M. J., and Nokes, R. I. (2007). "Inclined Negatively Buoyant Discharges." J. Hydraul. Eng., 10.1061/(ASCE)0733-9429(2007)133:5(545), 133(5), 545-554.

Lee, J. H. W., and Tang, H. W. (1999) "Experiments of a Duckbill Valve (DBV) Jet in Coflow." Proc., IAHR Congress, Graz, Austria, August 1999.

Palomar, P., Lara, J. L., Losada, I. J., Rodrigo, M., and Alvárez, A. (2012a). "Near field brine discharge modelling part 1: Analysis of commercial tools." Desalination, 10.1016/j.desal.2011.11.037, 290(0), 14-27.

Palomar, P., Lara, J. L., and Losada, I. J. (2012b). "Near field brine discharge modeling part 2: Validation of commercial tools." Desalination,

10.1016/j.desal.2011.10.021, 290(0), 28-42.

Roberts, P. J. W., and Abessi, O. (2014). "Optimization of Desalination Diffusers Using Three-Dimensional Laser-Induced Fluorescence: Final Report. Prepared for United States Bureau of Reclamation." School of Civil and Environmental Engineering, Georgia Institute of Technology, January 22, 2014.

Roberts, P. J. W., Snyder, W. H., and Baumgartner, D. J. (1989). "Ocean Outfalls. I: Submerged Wastefield Formation." J. Hydraul. Eng., 115(1), 1-25.

Roberts, P. J. W., Ferrier, A., and Daviero, G. J. (1997). "Mixing in Inclined Dense Jets." J. Hydraul. Eng., 123(8), 693-699.

Roberts, P. J. W., Salas, H. J., Reiff, F. M., Libhaber, M., Labbe, A., and Thomson, J. C. (2010). Marine Wastewater Outfalls and Treatment Systems, International Water Association, London.

Shao, D., and Law, A. W.-K. (2011). "Boundary impingement and attachment of horizontal offset dense jets." Journal of Hydro-Environment Research, 10.1016/j.jher.2010.11.003, 5(1), 15-24.

SCCWRP (2012). "Management of Brine Discharges to Coastal Waters Recommendations of a Science Advisory Panel." Southern California Coastal Water Research Project, Technical Report 694, March 2012.

SWRCB (2015). "Water Quality Control Plan Ocean Waters of California." State Water Resources Control Board, California Environmental Protection Agency, Sacramento, California, Adopted May 6, 2015, Effective January 28, 2016.

Tian, X., and Roberts, P. J. W. (2003). "A 3D LIF System for Turbulent Buoyant Jet Flows." Expts. Fluids, 35, 636-647.

Tian, X., Roberts, P. J. W., and Daviero, G. J. (2004). "Marine Wastewater Discharges from Multiport Diffusers I: Unstratified Stationary Water." J. Hydraul. Eng., 130(12), 1137-1146.

Tenera (2014). "Draft Moss Landing Desalination Plant Intake Impact Assessment: Larval Entrainment." Prepared for DeepWater Desal by Tenera Environmental, San Luis Obispo, CA 93401.

Trussell Technologies (2016) "Minimum Dilution Requirements." Memorandum June 9, 2016.

Walter, R. K., Squibb, M. E., Woodson, C. B., Koseff, J. R., and Monismith, S. G. (2014). "Stratified turbulence in the nearshore coastal ocean: Dynamics and evolution in the presence of internal bores." *Journal of Geophysical Research: Oceans*, 10.1002/2014jc010396, 119(12), 8709-8730.

Webster, D. R., Roberts, P. J. W., and Ra'ad, L. (2001). "Simultaneous DPTV/PLIF measurements of a turbulent jet." *Expts. Fluids*, 30, 65-72.

Wygnanski, I. and Fiedler, H.E. (1969). "Some Measurements in the Self-Preserving Jet." Journal of Fluid Mechanics 38(3): 577-612.

APPENDIX A. DIFFUSER HYDRAULICS WITH CHECK VALVES

1. Introduction

The calculation procedure to predict the internal hydraulics and flow distribution for diffusers with ports equipped with check valves is described below.

2. Check Valves

Typical check valves similar to those installed on the MRWPCA outfall are shown in Figure A-1. As the flow though the valve increases, the opening area increases, up to some limit. The valves attached to the MRWPCA outfall are four-inch flange TideFlex TF-2, Series 35, Hydraulic Code 61. The characteristics of the valves were provided by the manufacturer, TideFlex, Inc. and are shown in Figure A-2. The main characteristics are total head loss, jet velocity, and effective opening area as functions of flow rate.

Figure A-1. Typical "Duckbill" Check Valves

The relationship $E' = f(Q_j)$ between the total head, E' and flow Q_j of Figure A2 over the flow range 50 to 300 gpm can be closely approximated by the linear relationship:

$$E' = 0.020 Q_j - 0.276 \tag{A1}$$

where E' is the head in feet, and Q_j the flow rate in gpm. Similarly, the jet velocity (in ft/s) can be approximated by:

$$V_j = -4.71 \times 10^{-5} Q_j^2 + 6.49 \times 10^{-2} Q_j + 4.28 \tag{A2}$$

The effective nozzle area A_j is then given by:

$$A_j = \frac{Q_j}{V_j}$$

and the diameter of an equivalent round nozzle, d_e by:

$$d_e = \sqrt{\frac{4A_j}{\pi}} \tag{A3}$$

Therefore, only the relationship between head and flow, Eq. A1, and flow and velocity, Eq. A2, are needed and all other properties can be calculated from them. Alternatively, the equivalent diameter can be calculated from the flow and head assuming a discharge coefficient of one.

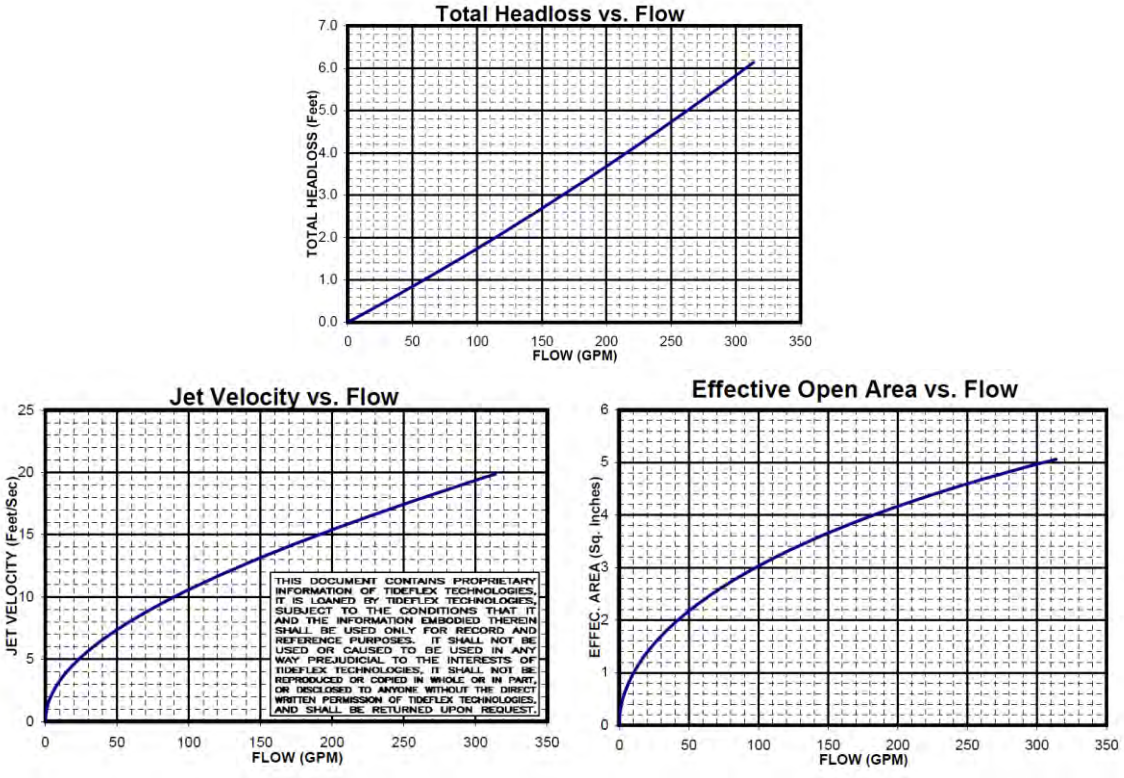

Figure A-2. Characteristics of 4" wide bill TideFlex check valve Hydraulic Code 61

3. Port Head Loss

According to the outfall design drawings (Figure A-3), the check valves are fastened over existing two-inch diameter ports. The entrances to the ports are gradually tapered bell mouths.

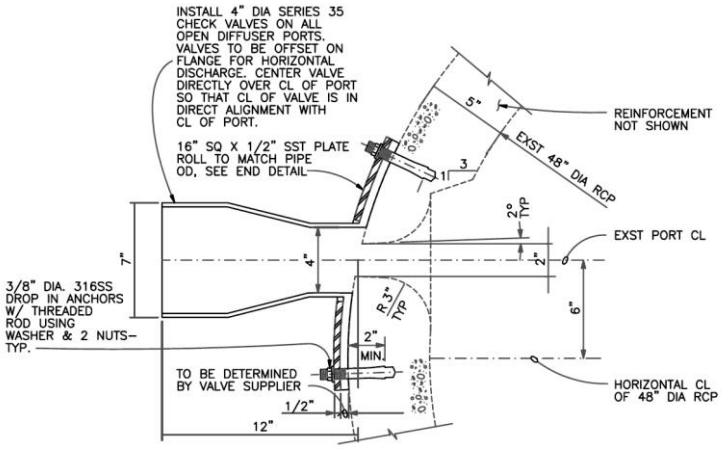

Figure A-3. Port and check valve arrangement

The head loss in the entrance from the diffuser to the port (entrance loss) can be approximated by:

$$h_f' = x_{en}\frac{V_d^2}{2g} \tag{A4}$$

where x_{en} is an entrance loss coefficient and V_d the velocity in the diffuser pipe at the port. The value of x_{en} is not known exactly, but experiments on Tee fittings reported by Ding et al. (2005) give loss coefficients for 6, 8, and 10 inch pipes with branching flows. For the larger Tees the loss coefficients ranging from about 0.43 to 0.63 depending on the ratio of flow in the branch to the main pipe. We assume a constant value of x_{en} = 0.63. Because the port entrances are rounded, and most of the head loss is in the jet velocity head, however, the results are not sensitive to the value of x_{en}.

Applying the Bernoulli equation to the flow through the port and valve and combining Eqs. A1 and A4 yields for the head at the port:

$$E = \text{Entrance loss} + \text{Valve loss}$$
$$= x_{en}\frac{V_d^2}{2g} + 0.020Q_j - 0.276$$

which can be rearranged as:

$$Q_j = \frac{E - x_{en}\left(V_d^2/2g\right) + 0.276}{0.02} \tag{A5}$$

4. End Gate Port

The end gate of the diffuser has an opening at the bottom as shown in Figure A-4. It is approximately 2 inches high in a 48-inch diameter pipe which corresponds to an area of 25.8 in^2, equivalent to a round opening of 5.73 inch diameter.

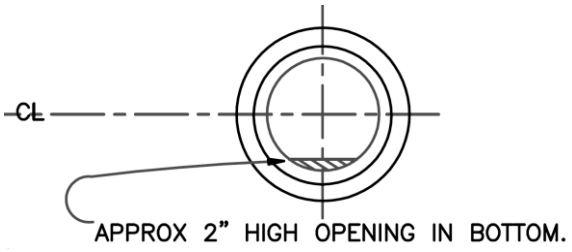

Figure A-4. End gate opening.

We approximate the discharge though this opening as being equivalent to a round sharp-edged orifice:

$$Q = C_D A\sqrt{2gE} \tag{A6}$$

where C_D is the discharge coefficient assumed equal to 0.62, A is the opening area and E the total head in the pipe just upstream of the end gate.

5. Diffuser and Pipe Head Loss

The head loss due to friction in the diffuser and outfall pipe can be approximated by the Darcy-Weisbach equation:

$$h_f = f\frac{L}{D}\frac{V_d^2}{2g} \tag{A7}$$

where L is the pipe length, D the pipe diameter, and f the pipe friction factor, given by:

$$f = f\left(\mathrm{Re}, \frac{k}{D}\right) \tag{A8}$$

where Re is the Reynolds number, $\mathrm{Re} = V_d D/\nu$ where ν is the kinematic viscosity and k the equivalent roughness height. The friction factor can be obtained from the Moody diagram, but for computational purposes it is more convenient to estimate it from:

$$f = \frac{0.25}{\left[\log\left(\frac{k/D}{3.7} + \frac{5.74}{\mathrm{Re}^{0.9}}\right)\right]^2} \tag{A9}$$

Generally accepted values of *k* for concrete pipe range from 0.012 to 0.12 inches. We assume an average value of *k* = 0.066 inches.

6. Calculation Procedure

The calculation procedure is a problem in manifold hydraulics and is iterative, similar to that described in described in Fischer et al. (1979) or Roberts et al. (2010). It follows this procedure:

1. Assume a value of the head just upstream of the end gate, E_1. Then compute the flow Q_1 through the end opening from Eq. A6.
2. Compute the velocity in the diffuser pipe just upstream.
3. Compute the pipe friction factor from Eq. A9.
4. Compute the head in the diffuser pipe at the next upstream port from:

$$E_2 = E_1 + f\frac{s}{D}\frac{V_d^2}{2g} + \frac{\Delta\rho}{\rho}\Delta z \qquad \text{(A10)}$$

where *s* is the port spacing, $\Delta\rho = \rho_a - \rho_o$ is the density difference between the receiving water and the discharge, ρ the receiving water density, and Δz the height difference between the ports (positive if the inshore port is higher, i.e. the diffuser is sloping downwards). Note that for a dense discharge, $\Delta\rho$ is a negative number.

5. Compute the flow from the next upstream port, Q_2, from Eq. 1.
6. Add the flows Q_1 and Q_2 to get the flow in the diffuser just upstream of the port.
7. Repeat steps 2 through 6 for each port until the innermost port is reached.

Finally, the head loss in the rest of the outfall pipe up to the headworks is computed from

$$E = E_n + f\frac{L}{D}\frac{V_d^2}{2g} + \text{density head}$$

where E_n is the head at the innermost port, *n,* and *L* is the outfall length (excluding the diffuser).

The total flow and head loss in the outfall are not known ahead of time, so the assumed head is Step 1 is then adjusted iteratively until the desired flow is achieved. An Excel spreadsheet was written to accomplish these calculations. A typical page from the spreadsheet for scenario P2 (pure brine) follows. For this example, the flow per port increases in the offshore direction due to the negative density head (dense brine discharge).

The total head for this case is essentially zero. This seemingly counterintuitive result is because the density head essentially offsets the losses due to friction and jet velocity.

Compute port flow distribution and total headloss with check valves

Tideflex Series TF-2, 35

Inputted variables

No. ports per riser, Nr =	**1**	Outfall pipe length, L (ft) =	**10,274**
Port spacing, Sr (ft) =	**8**	Roughness height, ks (in) =	**0.066**
Depth of end port, Hend (ft) =	**107**	Gravity, g (ft2/s) =	**32.2**
Slope of diffuser, Sl =	**0.0110**	Ambient density (kg/m3)	**1025.8**
Entrance loss coeff, xen =	**0.63**	Effluent density (kg/m3)	**1045.2**
		Density difference, Drho/rho =	**-0.019**
		Kinematic viscosity, nu (ft2/s) =	**1.2E-05**

Head at end:	**1.26**	ft	Outfall friction headloss:	0.81 ft
Target flow:	**14.0**	mgd	Diffuser headloss:	1.11 ft
Computed flow:	**14.0**	mgd	Density head:	-1.81 ft
			Total outfall head:	**0.11** ft

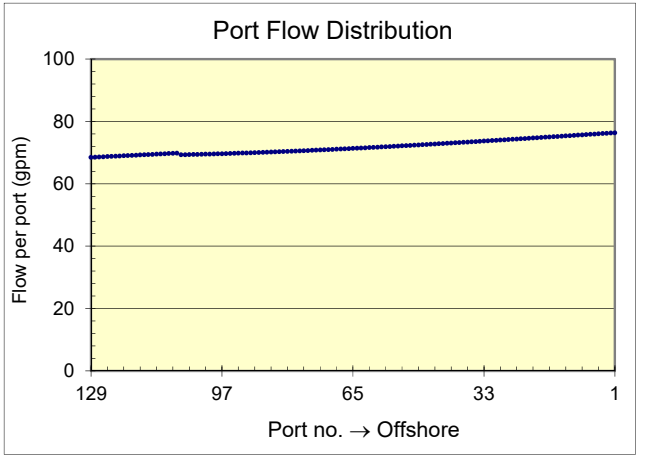

Pipe segment	Pipe ID	Port number	Distance from end	Depth	Total head	Flow				Velocity		Equivalent round port		Reynolds no.	Friction factor	Friction loss
						Per port	Per riser	Cumulative		Pipe	Jet	Diam.	Froude			
	(in)	n	(ft)	(ft)	(ft)	(gpm)	(gpm)	(gpm)	(ft3/s)	(ft/s)	(ft/s)	(in)				(ft)
End port					1.26	457	457	457	1.0	0.1	5.7	5.73	10.5			
1	48	1	0	107.0	1.26	76.3	76	533	1.2	0.1	9.0	1.87	29.1	3.1E+04	0.027	0.000
		2	8	106.9	1.26	76.3	76	609	1.4	0.1	9.0	1.87	29.1	3.6E+04	0.026	0.000
		3	16	106.8	1.26	76.2	76	686	1.5	0.1	9.0	1.87	29.1	4.0E+04	0.026	0.000
		4	24	106.7	1.26	76.1	76	762	1.7	0.1	8.9	1.86	29.1	4.5E+04	0.026	0.000
		5	32	106.6	1.25	76.0	76	838	1.9	0.1	8.9	1.86	29.1	4.9E+04	0.025	0.000
		6	40	106.6	1.25	75.9	76	914	2.0	0.2	8.9	1.86	29.1	5.4E+04	0.025	0.000
		7	48	106.5	1.25	75.8	76	990	2.2	0.2	8.9	1.86	29.0	5.8E+04	0.025	0.000
		8	56	106.4	1.25	75.8	76	1065	2.4	0.2	8.9	1.86	29.0	6.2E+04	0.025	0.000
		9	64	106.3	1.25	75.7	76	1141	2.5	0.2	8.9	1.86	29.0	6.7E+04	0.024	0.000
		10	72	106.2	1.25	75.6	76	1217	2.7	0.2	8.9	1.86	29.0	7.1E+04	0.024	0.000
		11	80	106.1	1.24	75.5	76	1292	2.9	0.2	8.9	1.86	29.0	7.6E+04	0.024	0.000
		12	88	106.0	1.24	75.4	75	1367	3.0	0.2	8.9	1.86	29.0	8.0E+04	0.024	0.000
		13	96	105.9	1.24	75.3	75	1443	3.2	0.3	8.9	1.86	29.0	8.5E+04	0.024	0.000
		14	104	105.9	1.24	75.3	75	1518	3.4	0.3	8.9	1.86	29.0	8.9E+04	0.024	0.000
		15	112	105.8	1.24	75.2	75	1593	3.6	0.3	8.9	1.86	29.0	9.3E+04	0.024	0.000
		16	120	105.7	1.24	75.1	75	1668	3.7	0.3	8.9	1.86	28.9	9.8E+04	0.024	0.000
		17	128	105.6	1.23	75.0	75	1743	3.9	0.3	8.9	1.86	28.9	1.0E+05	0.024	0.000
		18	136	105.5	1.23	74.9	75	1818	4.1	0.3	8.9	1.86	28.9	1.1E+05	0.023	0.000

APPENDIX B. DENSITY PROFILES

The seasonally averaged density profiles assumed for modeling purposes are summarized below.

Depth (m)	Density (kg/m^3)		
	Upwelling	Davidson	Oceanic
1	1025.1	1024.8	1024.8
3	1025.1	1024.8	1024.8
5	1025.1	1024.8	1024.8
7	1025.2	1024.8	1024.8
9	1025.2	1024.8	1024.8
11	1025.3	1024.8	1024.8
13	1025.4	1024.8	1024.9
15	1025.4	1024.8	1024.9
17	1025.5	1024.8	1024.9
19	1025.6	1024.9	1024.9
21	1025.6	1024.9	1025.0
23	1025.7	1024.9	1025.0
25	1025.7	1024.9	1025.0
27	1025.8	1024.9	1025.1
29	1025.8	1024.9	1025.1
31	1025.8	1024.9	1025.2
33	1025.9	1024.9	1025.2
35	1025.9	1024.9	1025.3

APPENDIX C. TURBULENCE EFFECTS ON ORGANISMS

Summary of lab and field data (and some models) regarding the effects of turbulence on organisms (from Foster et al. 2013).

Organism	Shear stress or turbulence	Method of generating shear/turbulence	Magnitude of critical shear/turbulence	Effect	Reference	Additional notes
Sea urchin S. purpuratus larvae (3 day; prism)	Laminar shear	Couette flow[1], short term (30 min)	No deleterious effect with $\varepsilon \leq 1$ cm^2/s^3	Change in prey encounter rate	Maldonaldo and Latz (2011)	Neg eff cd be due to erosion of hydromech signal, or if local velocity faster than catch speed, reaction time. Mortality was 19% for the 0.1 cm^2/s^3, 22% for the 0.4 cm^2/s^3, and 53% for the 1 cm^2/s^3 flow treatments compared to 5% for the still control.
		Couette flow Long term (8 days of 12 h on, 12 h off)	$\varepsilon < 0.1$ cm^2/s^3	Excessive mortality		
Sea urchin L. pictus larvae (3 day, 4 arm pluteus)	Laminar shear	Couette flow[1], short term (30 min)	No deleterious effect with $\varepsilon \leq 1$ cm^2/s^3	Change in prey encounter rate	Maldonaldo and Latz (2011)	
		Couette flow Long term (8 days of 12 h on, 12 h off)	No deleterious effect with $\varepsilon \leq 1$ cm^2/s^3	Some mortality, but not much		
Sea urchin S. purpuratus	Shear stress	Couette flow (short term: 2 min)	No deleterious effect with $\varepsilon < 200$ cm^2/s^3	Fertilization and development to blastula	Mead and Denny 1995, Denny, Nelson and Mead 2002	
Zebra mussel Dreissena polymorpha veliger	Turbulence	Bubble plume for 24 hours, then 24 feed before mortality measured	Mortality increases when d* > 0.9 (eddy similar in size to larva (no sig eff when d*<0.9)	Mortality	Rehmann et al. 2003	

Organism	Shear stress or turbulence	Method of generating shear/turbulence	Magnitude of critical shear/turbulence	Effect	Reference	Additional notes
dinoflagellate Alexandrium fundyense	Laminar shear	Couette flow for 1-24 hours/day	Shear stress τ = 0.003 N/m^2 ; $\varepsilon = 10^{-5}$ cm^2/s^3 ; only 1 level	Growth rate decreased when exposed to τ for more than 2 hours/ day	Juhl et al. 2001	Growth rate = 0 when shear 12 h/d; negative when 16-24 h/day
dinoflagellate Alexandrium fundyense	Laminar shear and turbulence	Couette flow 1 h/d 5–8 d and shaken flasks	Shear stress τ = 0.004 N/m^2 (not quantified for shaken flasks	Growth rate decreased in both	Juhl et al. 2000	Most sensitive last hour of dark phase, under lower light conditions
dinoflagellate Lingulodiniu m polyedrum.	Shear (steady and unsteady)	Couette flow; constant or changing speeds/direction; 2 h/d (change ev 2 min)	smallest ε = 0.04 cm^2/s^3; all had effect (very very high)	Growth rate decreased in all cases; often catastrophicall y (near 100%)	Latz et al. 2009	Unsteady flow had more of an effect than steady, even when mean was lower; poss mechanism: mechanical energy of the flow alters membrane biophysical properties, activates signal transduction pathway involving GTP, [ca2+]I, poss. Also involves cyclin-dep kinases, as in endothelial cells
Copepod Acartia tonsa	Turbulence	model	Starts dropping at $\varepsilon = 10^{-3}$ cm^2/s^3	Decrease in prey capture success	Kiørboe and Saiz 1995	Copepods that set up feeding currents are largely independent of ambient fluid velocity for prey encounters, while ambush-preying copepods can benefit substantially
Copepod Acartia tonsa	Turbulence	Oscillating grid			Saiz & Kiørboe 1995	
Herring larvae	Turbulence	model	Starts dropping at $\varepsilon = 10^{-3}$ cm^2/s^3	Decrease in prey capture success	Kiørboe and Saiz 1995	
Cod larvae	Turbulence	model	Starts dropping at $\varepsilon = 10^{-5}$ cm^2/s^3	Decrease in prey capture success	Kiørboe and Saiz 1995	

Organism	Shear stress or turbulence	Method of generating shear/turbulence	Magnitude of critical shear/turbulence	Effect	Reference	Additional notes
Cod Gadus morhua (5-6 mm)	Turbulence	Oscillating grid; observations start after 10 min shaking	$\varepsilon = 7.4 \times 10^{-4}$ cm^2/s^3)	Increase in "attack position rate" at all conc	MacKenzie and Kiørboe 1995	Cod benefit more from turb (pause-travel)
Cod Gadus morhua (8.7-12.3 mm)	Turbulence -more intermitten t	Oscillating grid, observations start after a few min shaking	$\varepsilon = .2, 2 \times 10^{-4}$ cm^2/s^3)	While encounter rate up, pursuit success down	MacKenzie and Kiorboe 2000	Decrease in pursuit success at higher ε; general downward trend with increased rel vel; smaller fish larvae affected more
Herring Clupea harengus (8-9 mm)	Turbulence	Oscillating grid; observations start after 10 min shaking	$\varepsilon = 7.4 \times 10^{-4}$ cm^2/s^3)	Increase in "attach position rate" only at low conc; v messy data	MacKenzie and Kiorboe 1995	Herring benefit less (cruise)
Juvenile rainbow trout and steelhead Oncorhynchus mykiss, Chinook salmon O. tshawytscha, American shad Alosa sapidissima	Shear stress	Forced entry directly into submerged jet in flume having exit velocities of 0 to 21.3 m/s	No effect at 168/s 341/s; LC-10 estimated at 495/s	Torn opercula, missing eyes	Nietzel et al. 2004	LC-10 =affects 10% of population Juvenile fish 83-232 mm fork length
Water flea Daphnia pulex	Turbulence	Vibrating 0.5 cm grid	$\varepsilon = 0.05$ cm^2/s^3 (as compared to calm)	Heart rate increased 5-27%	Alvarez et al. 1994	HR reflects increase in metabolic rate?
Copepod Calanus gracilis	Turbulence	Vibrating 0.5 cm grid	$\varepsilon = 0.05$ cm^2/s^3 (as compared to calm)	Heart rate increased 93%	Alvarez et al. 1994	Other species too including crab larvae (increase HR 9%)
Copepod Acartia tonsa	Turbulence	Oscillating grid	$\varepsilon = 0.001$ cm^2/s^3 (as compared to calm)	Decreases predator sensing ability	Gilbert and Buskey 2005	

Organism	Shear stress or turbulence	Method of generating shear/turbulence	Magnitude of critical shear/turbulence	Effect	Reference	Additional notes
Copepod Acartia tonsa	Turbulence (field)	Boat wake (field); plankton tow inside/ outside wake	ε =310 cm^2/s^3 at a distance of 50 propeller diam. behind 20 mm diam, scale-model boat propeller running at 3000 rpm	More dead inside wake (5-25% increase, over 2-12% background)	Bickel et al. 2011	Stain w neutral red
Copepod Acartia tonsa		Mini stirrer w paddles (lab)	ε = 0, 0.035, 1.31, 2.24 cm^2/s^3		Bickel et al. 2011	ε = 0.035 cm^2/s^3 did not show negative effect
Various	Turbulence (field)	Rapids (samples collected above and below rapids	ε = 3-742 cm^2/s^3	Effects dep on species: sign. mortality in Littorina littorea, Mytilus edulis, and Aporrhais pespelicant	Jessop 2007	Mytilus membranipora, Electra pilosa, polychaete trochophores and Lamellaria perspicua had zero mortality

ε = energy dissipation rate (cm^2/s^3)

Couette flow: two concentric cylinders, outer one rotates shearing volume of fluid between cylinders at known rate

Bibliography

Alcarez, M., E. Saiz, & A. Calbet. (1994). Small-scale turbulence and zooplankton metabolism: Effects of turbulence on heartbeat rates of planktonic crustaceans. Limnol. Oceanogr., 39(6), 1994, 1465-1470

Bickel, S. L., J. D. M. Hammond, & K. W. Tang (2011). Boat-generated turbulence as a potential source of mortality among copepods. Journal of Experimental Marine Biology and Ecology 401: 105–109

Bruton, M. N. (1985). The effects of suspensoids on fish. *Hydrobiologia* 125: 221-241.

Chesney, E. J., Jr (1989). Estimating the food requirements of striped bass larvae *Morone saxatilis:* effects of light, turbidity and turbulence. Mar. Ecol. Prog. Ser. Vol. 53: 191-200.

Dauvin, J.-C. and J. J. Dodson (1990) Relationship between feeding incidence and vertical and longitudinal distribution of rainbow trout larvae (*Osmerus mordax*) in a turbid, well-mixed estuary. Mar. Ecol. Prog. Ser. Vol. 60: 1-12.

Einav, R., K. Hamssib, D. Periy (2002). The footprint of the desalination processes on the environment. Desalination 152 (2002) 141-154

Evans, M. S. (1981). Distribution of zooplankton populations within and adjacent to a thermal plume. Can. J. Fish. Aquat. Sci. 38: 441-448.

Huang, S., N. Voutchkov, S. C. Jiang (2013). Investigation of environmental influences on membrane biofouling in a Southern California desalination pilot plant. Desalination 319: 1–9

Jessopp, M. J. (2007) The quick and the dead: larval mortality due to turbulent tidal transport. J. Mar. Biol. Ass. U.K. 87, 675-680.

Jones, I. S. F. & Y. Toba [EDS.]. (2001) Wind stress over the ocean. Cambridge Univ. Press.

Juhl, A. R., V. Velasquez, M. I. Latz (2000) Effect of growth conditions on flow-induced inhibition of population growth of a red-tide dinoflagellate. Limnol Oceanogr 45:905–915

Juhl, A. R., V. L. Trainer, M. I. Latz (2001) Effect of fluid shear and irradiance on population growth and cellular toxin content of the dinoflagellate *Alexandrium fundyense.* Limnol Oceanogr 46: 758–764

Kiørboe, T., E. Saiz (1995) Planktivorous feeding in calm and turbulent environments, with emphasis on copepods. Mar Ecol Prog Ser 122: 135–145.

Latz, M.I., J. Allen, S. Sarkar, J. Rohr (2009) Effect of fully characterized unsteady flow on population growth of the dinoflagellate *Lingulodinium polyedrum.* Limnol Oceanogr 54:1243–1256.

Lunz, R. G. (1938). Part I. Oyster culture with reference to dredging operations in South Carolina. Part II. The effects of the flooding of the Santee River in April 1936 on oysters in the Cape Romain area of South Carolina. Report to U. S.

Engineer Office, Charleston, South Carolina, 1-33.

MacKenzie, B. R. and T. Kiørboe (1995). Encounter rates and swimming behavior of pause-travel and cruise larval fish predators in calm and turbulent laboratory environments. Limnol. Oceanogr., 40(T), 1995, 1278-1289.

MacKenzie, B. R. and T. Kiørboe (2000). Larval fish feeding and turbulence: A case for the downside. Limnol. Oceanogr., 45(1), 2000, 1–10

Maldonado, E. M. and Latz, M.I. (2011) Species-specific effects of fluid shear on grazing by sea urchin larvae: comparison of experimental results with encounter-model predictions. Mar Ecol Prog Ser 436:119-130

Mead, K. and Denny, M. (1995). Effects of hydrodynamic shear stress on the fertilization and early development of the purple sea urchin, *Strongylocentrotus purpuratus. Biol. Bull.* 188: 46-56.

Miner J.G., Stein R.A. (1996) Detection of predators and habitat choice by small bluegills: effects of turbidity and alternative prey. Trans Am Fish Soc 125:97±103

Peters F, C. Marrasé (2000). Effects of turbulence on plankton: an overview of experimental evidence and some theoretical considerations. Mar. Ecol. Prog. Ser. 205: 291–306,

Rehmann, C. R., J.A. Stoeckel, and D.W. Schneider (2003a). Effect of turbulence on the mortality of zebra mussel veligers. Can. J. Zool. 81: 1063–1069

Saiz, E., T. Kiørboe (1995). Predatory and suspension feeding of the copepod Acartia *tonsa* in turbulent environments. Mar. Ecol. Prog. Ser. 122: 147-158

SCCWRP (2012), Management of Brine Discharges to Coastal Waters Recommendations of a Science Advisory Panel," submitted at the request of the State Water Resources Control Board by the Southern California Coastal Water Research Project, Costa Mesa, CA, Technical Report 694, March 2012

Vinyard, G. L. and W. J. O'Brien (1976) Effects of Light and Turbidity on the Reactive Distance of Bluegill (*Lepomism acrochirus*) J. Fish. Res. Board Can. 13:2845-2849.